Mold Design Concept for Injection Molding of Highly Filled Compounds

Ing. Jakub Huba, Ph.D.

Doctoral Thesis Summary

Tomas Bata University in Zlín

Tomas Bata University in Zlín
Faculty of Technology

Doctoral Thesis Summary

Koncept vstřikovací formy pro vysoce plněné polymery

Mold Design Concept for Injection Molding of Highly Filled Compounds

Author: **Ing. Jakub Huba, Ph.D.**

Degree programme: P3909 Process Engineering

Degree course: 3909V013 Tools and Processes

Supervisor prof. Ing. Berenika Hausnerová, Ph.D.

External examiners: prof. Ing. Karel Kocman, DrSc.

prof. Dr. Ing. Vladimír Mostýn

Zlín, June 2019

Published by **Tomas Bata University in Zlín** in the Edition **Doctoral Thesis Summary.**
The publication was issued in the year 2019

Klíčová slova: vysoce plněné systémy, vstřikování, fázová separace, tokové analýzy, infračervené senzory, studené spoje, teplotní vodivost, počítačová tomografie, pevnost v tahu

Keywords: highly filled compound, injection molding, phase separation, filling simulation, infra-red sensors, weld line, thermal conductivity, computed tomography, tensile strength

Full text of the doctoral thesis is available in the Library of TBU in Zlín.

ISBN 978-80-7454-852-9

CONTENT

ABSTRACT

The thesis discusses the mold design for highly filled polymer melts, with a special emphasis on powder injection molding (PIM) compounds, which substantially differs from mold design requirements applied to conventional thermoplastic injection molding.

First part of the Thesis is devoted to a phase separation during injection molding. The mold design to quantify separation recently proposed by the PIM research group at TBU is treated with flow simulation approach (Moldflow). The data obtained from a capillary rheometry (viscosity) and differential scanning calorimetry (specific heat capacity) and modified transient plane source technique (thermal conductivity) is implemented to Cross model, where temperature-induced physical changes are predicted with the help of Williams-Landel-Ferry equation (WLF). Both models are used for simulations, and according to the results obtained, the new mold design is proposed. Simultaneously, the phase separation is detected with computed tomography on the real samples of stainless steel feedstock used in PIM.

As it is found that the separation is closely related to shear rate gradients accompanied with temperature changes, infra-red sensors are installed into the new testing mold to intercept the areas prone to this issue. Real observations made on PIM compounds are compared with simulated ones, and statistically analysed.

Second part of the Thesis is focused on a common problem during injection molding – weld line formation, which is most severe for highly filled polymers due to a lack of polymer entanglement across the approaching of the flow fronts. To increase time for an entanglement, the mold inserts from various materials (copper, aluminum, bronze, epoxy resin, and epoxy resin with hexagonal boron nitride, acrylic 3D printing material) with different thermal conductivity are used. It is shown (with the support of carefully selected statistical methods) that in case of conventional highly filled compounds as wooden plastic composites, weld lines have a considerable effect on the tensile strength, while for PIM feedstocks have not, but the presence of a weld line in a PIM part may be beneficial as it results in the shortening of the filling trajectory, and subsequently, leads to the time saving during molding.

ABSTRACT IN CZECH

Dizertační práce se zabývá koncepcí návrhu vstřikovacích forem pro vysoce plněné polymerní taveniny s důrazem na materiály pro práškové vstřikování (tzv. PIM technologii), kde se design nástrojů částečně liší v porovnání s požadavky pro vstřikování termoplastů.

První část práce je věnována fázové separaci, která vzniká během vstřikování vysoce plněných polymerních tavenin. Vstřikovací forma pro kvantifikaci fázové separace, jejíž konstrukci navrhla výzkumná skupina pro PIM na UTB ve Zlíně, byla podrobena tokové analýze (Moldflow). Získaná materiálová data pro výpočet viskozity, měrné tepelné kapacity a tepelné vodivosti byla implementována do simulace založené na viskozitním modelu Crosse. K predikci změny viskozity v závislosti na teplotě byl využit Williams-Landel-Ferry model. Z výsledků simulací byl odvozen návrh nové testovací geometrie. K detekci fázové separace na reálných PIM vzorcích na bázi nerezové ocele byla využita počítačová tomografie.

Bylo zjištěno, že fázová separace je úzce spjata s gradienty rychlosti smykové deformace. Jelikož jsou tyto gradienty doprovázeny změnou teploty, byla lokalizovaná kritická místa formy osazena infračervenými senzory pro měření teploty taveniny. Data získaná z měření byla porovnána s průběhy teploty během simulace procesu a statisticky vyhodnocena.

Druhá část práce pojednává o standardním problému během vstřikování – studeném spoji, což je v případě vysoce plněných polymerů (v důsledku nedostatečné difuze čel taveniny v místě studeného spoje) jeden z vážných problémů doprovázejících jejich zpracování. Pro prodloužení doby pro formování polymerních zapletenin byly použity vložky vstřikovací formy s různou tepelnou vodivostí (měď, hliník, bronz, epoxidová pryskyřice, epoxidová pryskyřice plněná hexagonálním nitridem bóru a akrylátová vložka z 3D tiskárny). V práci je statisticky podloženo, že v případě vysoce plněných polymerů na bázi tzv. WPC kompozitů, studené spoje mají značný vliv na pevnost, zatímco PIM směsi nevykazují žádnou závislost. V případě PIM materiálů však přítomnost studeného spoje zkracuje tokovou dráhu, což může vést k časové úspoře během vstřikovací fáze procesu.

INTRODUCTION

Currently, the aim of circular economy is to reduce the amount of generated waste, and recycle used materials. Therefore, thermoplastic composites are coming to the foreground, and filling of thermoplastic matrices approaches maximum values in terms of processability. This applies specially to powder injection molding (PIM) technology. These highly filled materials consist from two phases during injection molding, and their segregation may lead to deterioration of performance properties as mechanical and aesthetical. If the phase separation occurs, the part should not be passed to next processing, but regrind and used again.

Further, high loadings are associated to an abrasive wear, and therefore, special requirements on a surface quality of tools in contact with a melted compound. Wear is considered as most important parameter governing changes in a surface quality of not only tools, but also molded parts. Furthermore, physical properties such as viscosity and strength are affected by wear due to a change of surface energy, slip effect and roughness variations. All of these adjustments lead to a phase separation of feedstock components - powder and binder, which is currently the most severe issue of PIM technology. As a consequence, suitably designed tool at the beginning of its life-time may fail due to the progressive modifications during usage. So far, simulation approaches do not consider these changes. Therefore, simulation of formation of phase separation is a challenge starting with its detection during injection molding. Current methods focus largely on post-processing qualification (not quantification) of segregation, and no on-line method has been introduced so far.

Another weak point of design concept of molds for highly filled compounds are different mechanical properties obtained in longitudinal and traverse flow (processing) directions. Situation is dramatically changing with the presence of weld lines – the areas, where two or more flow fronts approach each other. Decreased weld line strength is due to insufficient diffusion between flow fronts, limited area of polymer macromolecules because of presence of filler and creation of V-notch due to entrapped air. Entanglement time between macromolecules may be elongated with lower cooling rate of polymeric melt what can be achieved with lower temperature gradient between polymeric melt and mold surface, or by adjustment of thermal conductivity of mold material.

THEORETICAL BACKGROUND

1. SIMULATIONS

During injection molding a variety of defects may occur. These defects could be caused by design, e.g. retraction from design recommendations, non-standard mold design or manufacturing out of tolerances. Prediction of defects using simulation tools should lead to optimization of design of part and tool as well as selection of proper molding conditions (Heaney, 2012).

1.1 Governing Equations

During the filling stage of molding process, a continuum approach is used to establish the system of governing equations. Mass and momentum conservation should be adopted with the assumption of incompressible melt flow and then the continuity equation is expressed as (Heaney 2012):

$$\frac{\partial u}{\partial x}+\frac{\partial v}{\partial y}+\frac{\partial w}{\partial z}=0$$

where *x, y, z* represents Cartesian coordinates and *u, v, w* are velocity components in an orthogonal coordination system. Navier-Stokes equations for molten feedstock should be described as:

$$\frac{\partial P}{\partial x}=\frac{\partial}{\partial z}\left(\eta\frac{\partial u}{\partial z}\right) \quad and \quad \frac{\partial P}{\partial y}=\frac{\partial}{\partial z}\left(\eta\frac{\partial v}{\partial z}\right) \quad and \quad \frac{\partial P}{\partial y}=0$$

where P is the pressure, η is the viscosity of the feedstock and z is the thickness of the flow domain.

In respect with injection molding of two-phase component, variation of concentrations of each phase will represent segregation effect during filling stage. Therefore, velocity of material is a function of velocity of each phase:

$$V_{ef}=\phi_s V_s+\phi_f V_f$$

where V_{ef}, V_s, V_f are effective velocity, velocity of solid phase and velocity of fluid phase, respectively and ϕ_s denotes to volume fraction of solid and ϕ_f is volume fraction of fluid phase (Barriere 2002).

During filling saturation conditions should be verified:

$$\phi_s+\phi_f=1 \quad and \quad \frac{\partial\phi_s}{\partial t}+\frac{\partial\phi_f}{\partial t}=0$$

According to precondition of incompressibility of both phases, densities remain constant and therefore, apparent density for each phase in the mixture is related to its volume fraction as:

$$\rho_s = \phi_s \rho_{s0} \qquad and \qquad \rho_f = \phi_f \rho_{f0}$$

where ρ_s and ρ_f are apparent densities of solid and fluid phase, respectively, and symbol *0* in density represents intrinsic densities of corresponding phase. Therefore, mass conservation should be verified by the flow of each phase:

$$\frac{\partial \rho_p}{\partial t} + \nabla.\left(\rho_p V_p\right) = 0$$

This approach is currently integrated into Sigmasoft simulation software (Thornagel 2010, Duretek 2017).

1.2 Numerical Simulations of Highly Filled Compounds Flow

Simulation of PIM process is an issue due to distinct properties in comparison with polymer (conventional injection molding) and metal powder (powder metallurgy). Many studies performed with the help of commercially available softwares as Moldex3D (Andrews 2010, Walale 2018), Moldflow (Kate 2016) and PIMsolver (Atre 2007) have been released without verification with experimental results.

Bilovol *et* al. (Bilovol, 2003a) compared three CAE programs to computational simulations of PIM injection molding, namely C-mold, Moldflow and ProCAST. The obtained results were compared with the experimental data. C-mold and Moldflow used Cross-WLF viscosity approximation, on the other hand ProCAST used Carreau-Yasuda viscosity model. The experiment showed that a wider part of the cavity is filled faster than narrower part. However, C-mold software has not assumed any hesitation of feedstock (Fig. 1).

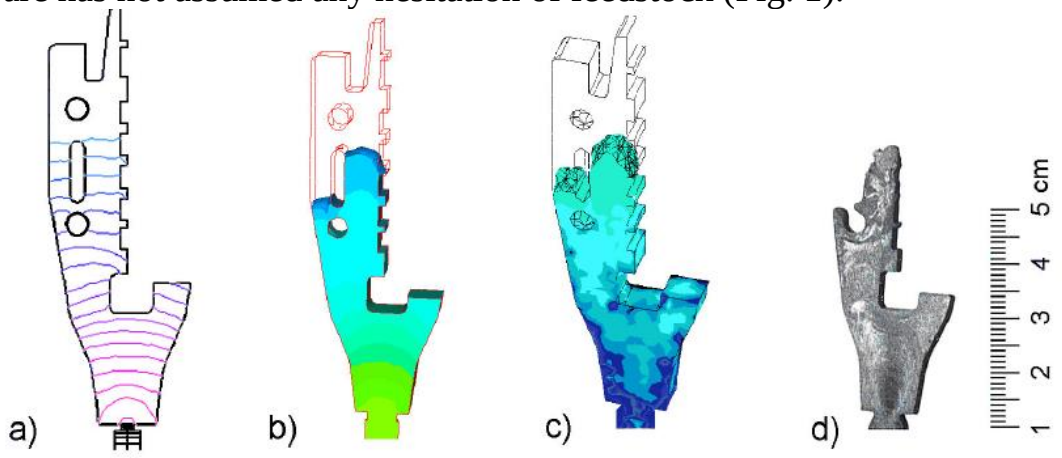

Fig. 1 - CAE simulation in C-mold (a), Moldflow (b), ProCAST (c), data from experiment (d) (Bilovov 2003a)

Bilovol (Bilovol, 2003b) also investigated a temperature distribution in CAE and compared it with real conditions. As a thermocouple, protruded Cr-Al type over cavity surface has been used. From the data obtained, it is evident that response time up to 0.5 s of bi-metal thermocouple leads to inaccurate data (position T3). C-mold predicts temperature development due to viscous flow and dissipation of shearing lead to increase of temperature between position T1 and T2 (Fig. 2). This phenomenon could be attributed to diameter of gating system (0.99 mm), where shear rate is predicted up to 5,000 s^{-1}. On the other hand, differences between T1 and T2 in ProCAST are not noticeable, and Moldflow ignores any viscous flow due to smooth decrease of temperature from gate to last filled location. Situation could be changed, if a finer mesh would be used.

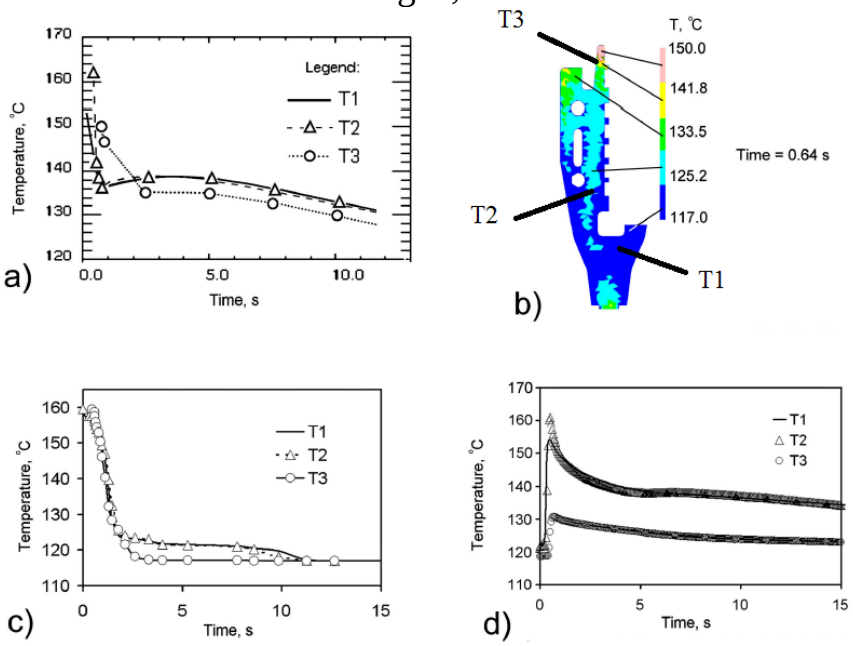

Fig. 2 - Prediction of temperature in C-mold (a), Moldflow (b), ProCAST (c) compared to real experiment (d) (Bilovol 2003b)

Drummer *et* al. (Drummer, 2014) compares flow front development in Sigmasoft software with experimental data. For his experiment, the first Newtonian plateau in Cross-WLF viscosity curve was substituted with Herschel-Bulkley viscosity model taking into account yield stresses (Fig. 3). This substitution has considerable influence, when the cavity is filled through a small gate, and presence of large surface of the melt with no contact to the mold wall is evident.

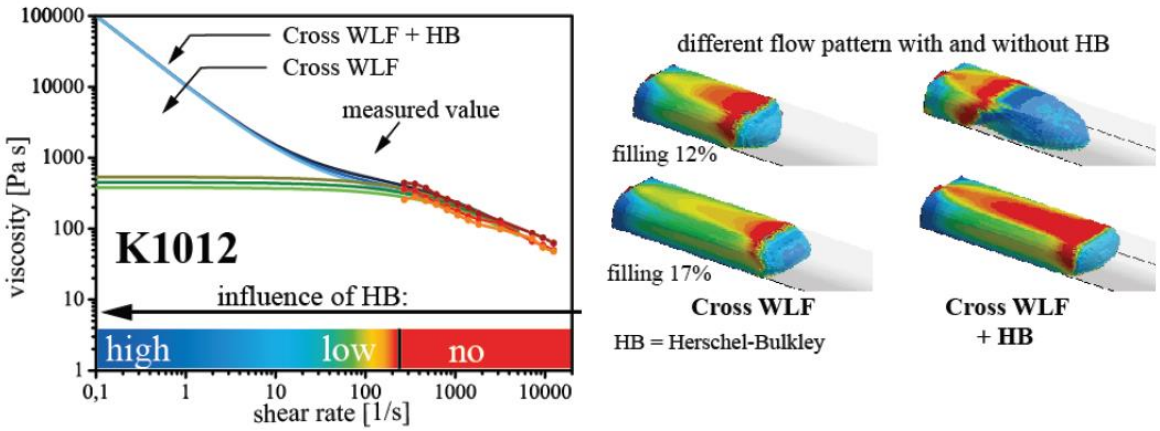

Fig. 3 - Replacement of the first Newtonian plateau from Cross-WLF with Herschel-Bulkley (Drummer 2014)

Marhöfer (Marhöfer, 2016) realized Moldflow simulation with comparison to experimental data. His investigation was focused on required pressure to fill the mold cavity. From results it is evident that requested pressure is approx. 20 % higher than predicted in Moldflow, and filling stage is about 45 % longer in comparison to Moldflow, Fig.4.

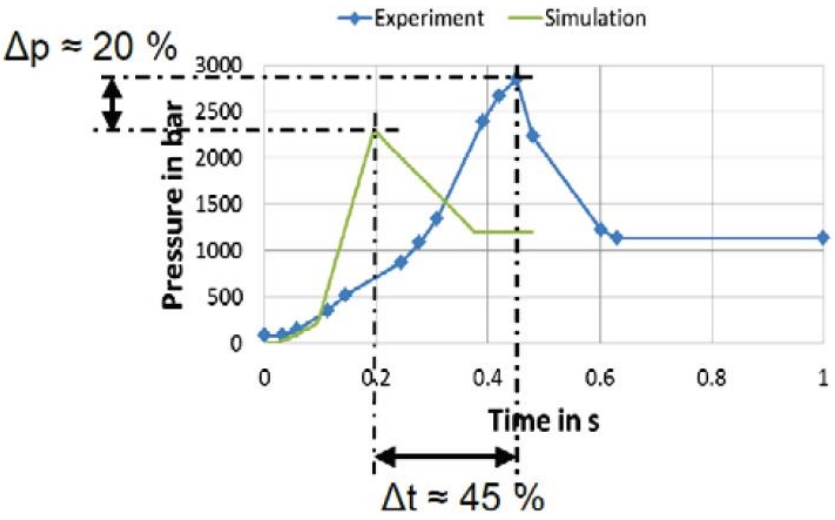

Fig. 4 - Injection pressure from Moldflow and real experiment (Marhöfer 2016)

This time extension might be caused by inertia of moving part of injection molding machine. On the other hand, Marhöfer (Marhöfer, 2016) operated with default thermal properties, and Moldflow is primary suitable for injection molding of plastics; typical thermal conductivity for plastics is λ_{PP} = 0.2 W.m^{-1}.K^{-1}, while for feedstocks it is 2,000 % higher ($\lambda_{17\text{-}4PH}$ = 4 W.m^{-1}.K^{-1}). Therefore, it is necessary to pay attention to material characteristics in order to minimize the error in input in boundary conditions in CAE software. Afterward, CAE simulations in PIM may be useful in the predictions of several problems during injection molding, and results may be incorporated in the tool design.

2. TOOLING

2.1. Tooling from Perspective of Moldability

Injection mold represents a complex task of production tools, where design engineering, material science, production engineering and quality control must be linked. Although design of injection mold for PIM feedstocks is similar to thermoplastic injection molding, few differences should be kept in mind during designing of the tool.

Generally, shrinkage in highly filled materials is rarely higher than 2 %, in PIM technology the final shrinkage after sintering step reaches the value between 15 % to 20 %. In some special applications as PSH PIM (Powder Space Holder Powder Injection Molding) to obtain porous structures with small porosity diameter, shrinkage may be up to 32 % (Heaney, 2012)

Shrinkage δ is calculated as a function of the length of the mold cavity L_0 and length of sintered part L:

$$\delta = \frac{L_0 - L}{L_0}$$

However, for a tool designer, it is more valuable to use a tool cavity expansion factor expressed as Z:

$$Z = \frac{L_0}{L} \quad \xrightarrow{or} \quad \frac{1}{1-\delta}$$

According to higher thermal conductivity of PIM feedstocks, obviously PIM injection molding machine has a longer nozzle than usual. The reason is due to minimizing of a sprue bushing length. Sprue bushing in thermoplastic injection molding works well with taper up to 1.5°, on the other hand, in PIM it is recommended to use taper of 5° due to stickiness of feedstock to the bushing surface. During injection molding, many occurring defects should be predicted with CAE simulations (entrapped air, weldlines, etc.). PIM powders are incompressible, and PIM feedstocks are more abrasive to the tools than thermoplastics. Therefore, parts in contact with a melted compound should be hardened or coated with wear resistant coating layers. Due to high filler volumes, injected parts are brittle and tend to stick to a parting line. Therefore, PIM tools should be produced in tighter tolerances in comparison with conventional injection molding to prevent flashing. Generally, in case of highly filled materials, mechanical properties may be significantly affected with weld line formation.

Xie *et* al. (Xie, 2010) molded PP matrix (DOW C705-44) filled with wood filler with 0.8 mm - 1.1 mm (Type 9) and 0.07 mm – 0.15 mm (type C100) particle

sizes,. Both fillers may be classified as fibers with different *L/D* ratios. Due to higher size of Type 9, filler particles cannot be well entangled and distributed in weld line area, and therefore, the negative effect on tensile strength is significant, Fig. 5.

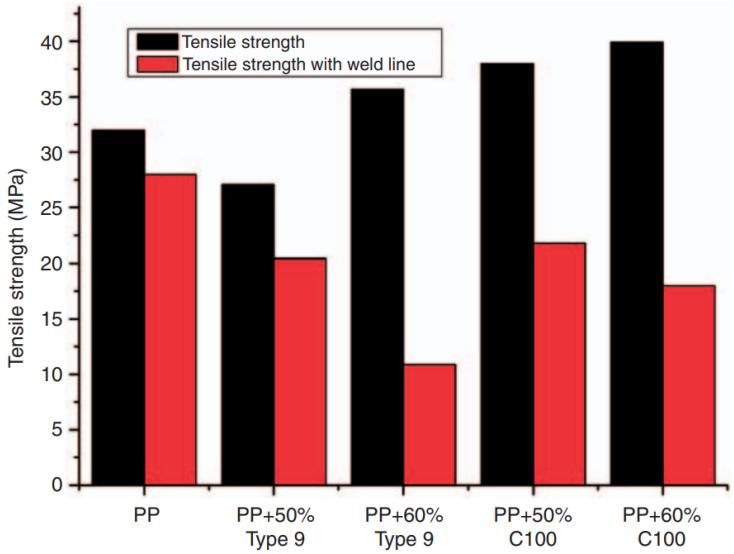

Fig. 5 - Influence of PP + fiber filler on tensile strength with/without weld line

Zhou *et* al. (Zhou, 2014) performed research on a flake filler. He used PP homopolymer with 40 wt.% of talc filler. From his results it is evident that flake filler has also negative effect on tensile strength, Fig.6.

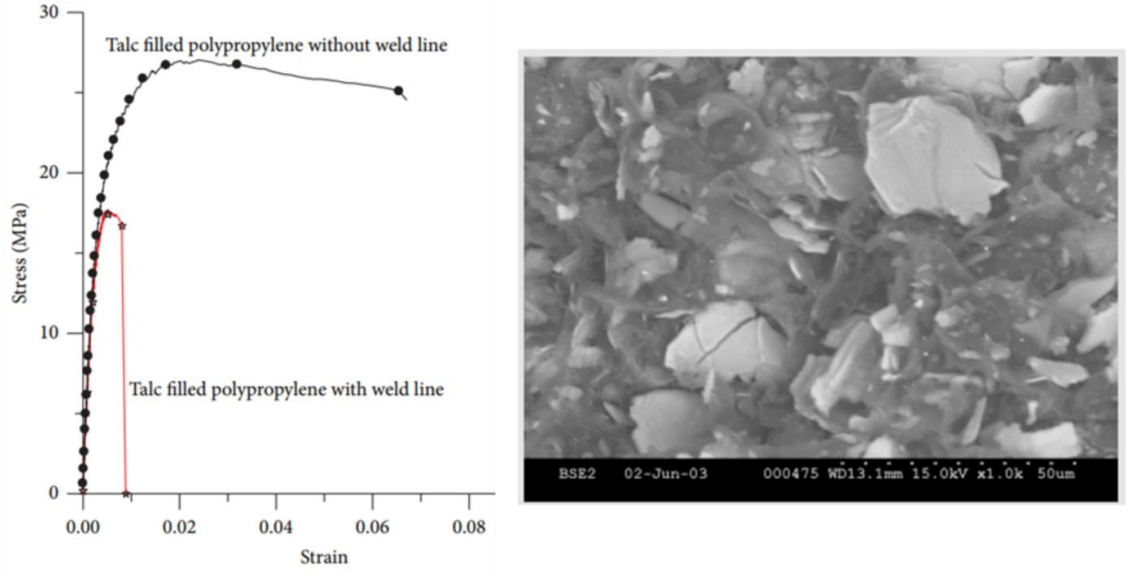

Fig. 6 - Influence of PP + flake filler on tensile strength with/without weld line

Chen *et* al. (Chen, 2007) published in his study effect of melt and mold temperature on overall tensile strength of ABS with and without weld line, Fig. 7. After photoelastic testing he found that increased melt and mold temperatures induce lower residual stresses in parts without weld line, and therefore, higher tensile strength can be reached. On the other hand, lower temperatures lead to

incomplete molecular diffusion of macromolecules in weld line area resulting in decreased tensile strength.

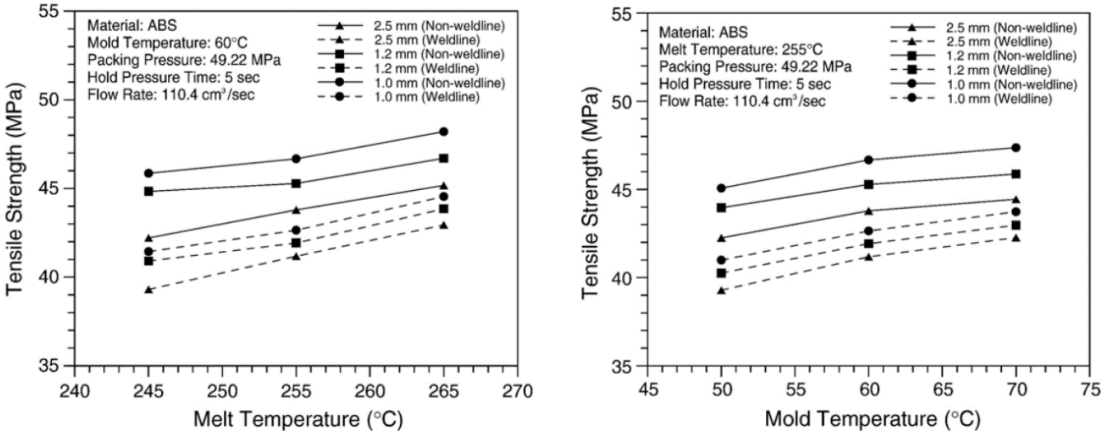

Fig. 7 - Effect of melt temperature on tensile strength with/without weld line (Chen, 2007)

Chookaew (Chookaew, 2018) investigated influence of mold temperature and distance from obstacle that forms weld line in rubber injection molding (Fig. 8) and showed that elevated temperature may positively affect weld line strength.

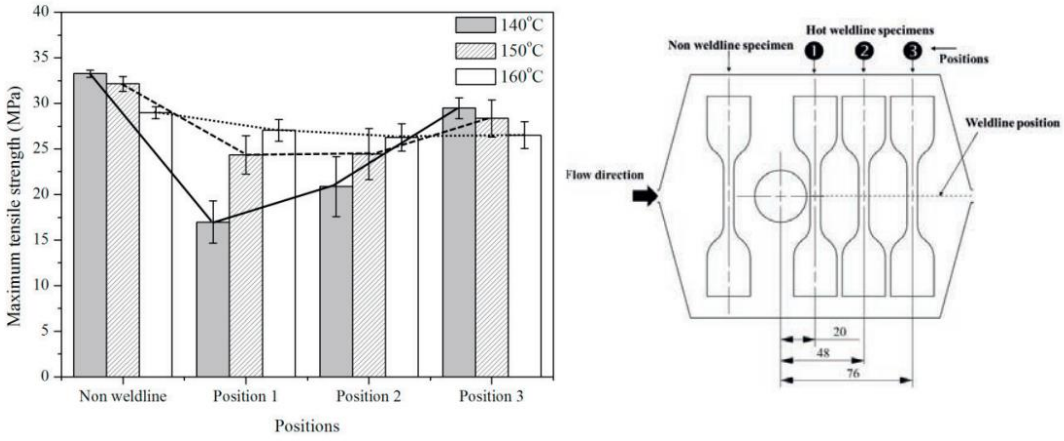

Fig. 8 - Effect of temperature and position of weld line on tensile strength for rubber injection molding (Chookaew, 2013)

Tensile strength of weld line depends on temperature. Thus, cooling rate has been investigated by Chen *et* al. (Chen, 2009) for ABS using different coatings of mold cavity, where PTFE is polytetrafluorethylene, TiN is titanium nitride and P20 is non-coated toolsteel (Fig. 9). Different coatings and different thicknesses of coatings have influence on tensile properties due to variation in the thermal conductivities and cooling rates. The values (in μm) 22, 10, 4 and 20, respectively, represent the thickness of the coating.

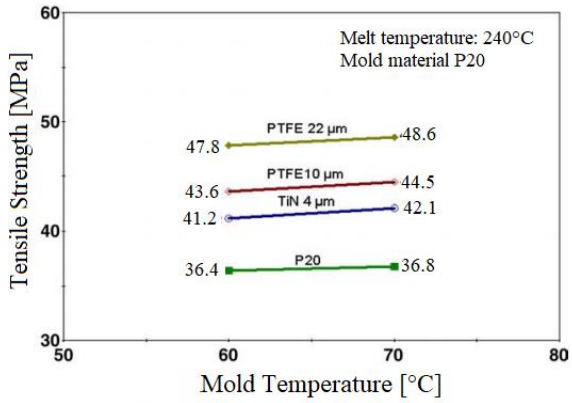

Fig. 9 – Weld line tensile strength with different thermal conductive interfaces (Chen 2009)

According to these findings, a present investigation will be focused on a weld line strength with different thermal conductivities of mold inserts, and an influence of processing parameters of highly filled compounds on a weld line strength.

According to high thermal conductivity of highly filled feedstocks in comparison to thermoplastics, a fast response of monitoring unit is necessary. Therefore, to monitor temperature. three methods are considered (Fig. 10).

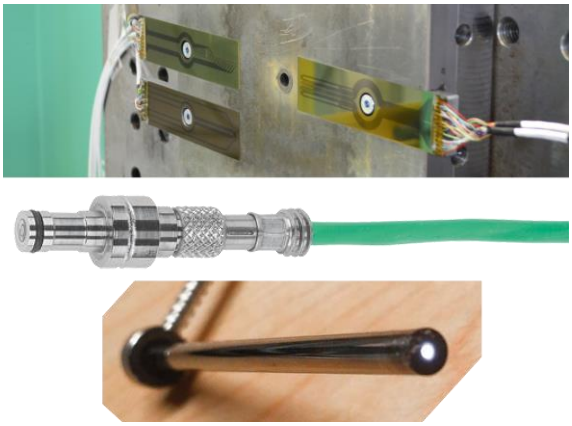

Fig. 10 - Thin film sensors (up) metal thermocouple (middle) infra-red sensor (bottom) (Kistler, 2019)

Thermocouple and thin-film sensors can be considered as contact measuring methods (Biehl, 2006, 2016, Kyas, 2012), on the other side infra-red (IR) temperature sensors are based on infrared radiation, and thus considered as non-contact measurements. From results of Martinsen *et* al. (Martinsen, 2017) it seems that the integrated thin film sensors are measuring surface temperature of the polymer surface. The same finding was reported by Guerrier *et* al. (Guerrier, 2017), where maximum temperature of ABS (217°C) during filling was recorded below T_g (70 °C). IR sensors monitor material temperature as a bulk with response time up to 10 ms. (Bendada, 2004)

3. PHASE SEPARATION OF HIGHLY FILLED COMPOUNDS

Powder/binder separation, in literature also referred as phase segregation, is the most frequently observed issue in PIM (German 1997, Heaney 2012, German 2013). Powder binder separation, created during injection molding stage, causes quality failure as uneven porosity, warpage, cracks or visual defects. The main factors influencing phase separation are different densities of feedstock components, high speed and high pressure of injection molding process (German 2011, Hausnerova 20111, Jenni 2008). Discussion with leading research institution in this area (Walcher 2013) revealed that the surface roughness finer than *R*a = 0.8 μm can be another cause of separation.

3.1. Theoretical Approach to Evaluation of Phase Separation

During injection molding stage it is necessary to have a homogenous mixture of powder and binder, and thus uniform distribution of a powder in feedstock granules. If this condition is accomplished, introducing of errors incoming from a mixing stage can be eliminated (Thornagel 2009).

Thornagel (Thornagel, 2009) demonstrated that during injection molding powder particles are forced by a local shear rate gradient to leave such areas of high shearing. As it is shown in Fig. 11, the particles in the middle of the flow domain within the plateau of shear rate continue their way without the change in the direction. The particles, which flow in the areas of the non-plateau shear rate gradients, are forced to rotate. The rotation becomes the bigger, the bigger the shear rate gradient is. Then, a change in the flow direction of the particles is initiated due to their rotation (Hausnerova 2011b, Thornagel 2009).

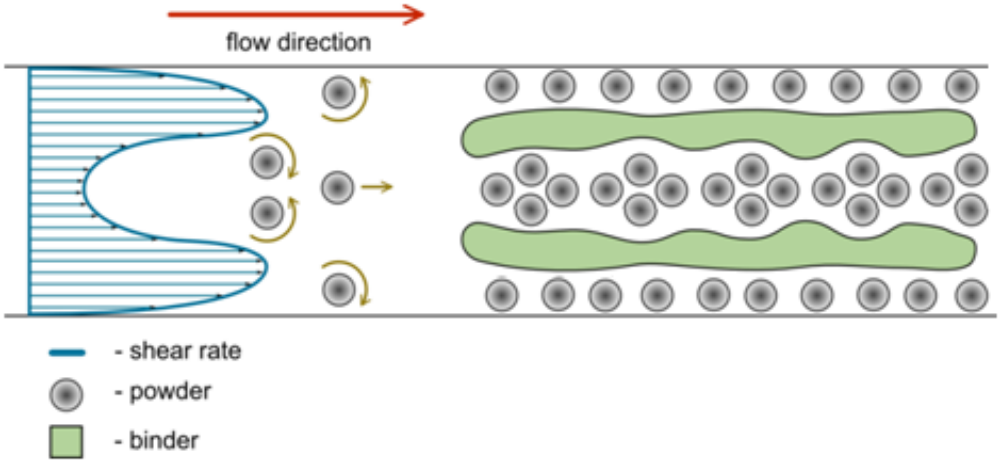

Fig. 11– Powder/binder separation caused by local shear rate gradients (Thornagel 2009)

Development of shear rate gradients is governed by a design of a mold cavity. Thus, the mold design plays the crucial role in the description of this issue. During the filling stage, a feedstock has a certain powder and binder contents because of low shear rate gradients in a runner system. The situation changes, when the volume unit arrives to the gate area, where the shear rate gradients become higher. According to the concept of separation (Fig. 12), the volume unit travelling in the center of the trajectory, will assign an additional powder. The volume unit flows through low and high shear rate areas to the final destination inside the mold cavity. During the flow, the perceptual content of powder particles is varying, and a phase separation occurs. It should be mentioned that the sudden changes in the flow direction can also cause phase separation and form powder rich areas (Karatas 2008, Heaney, 2012).

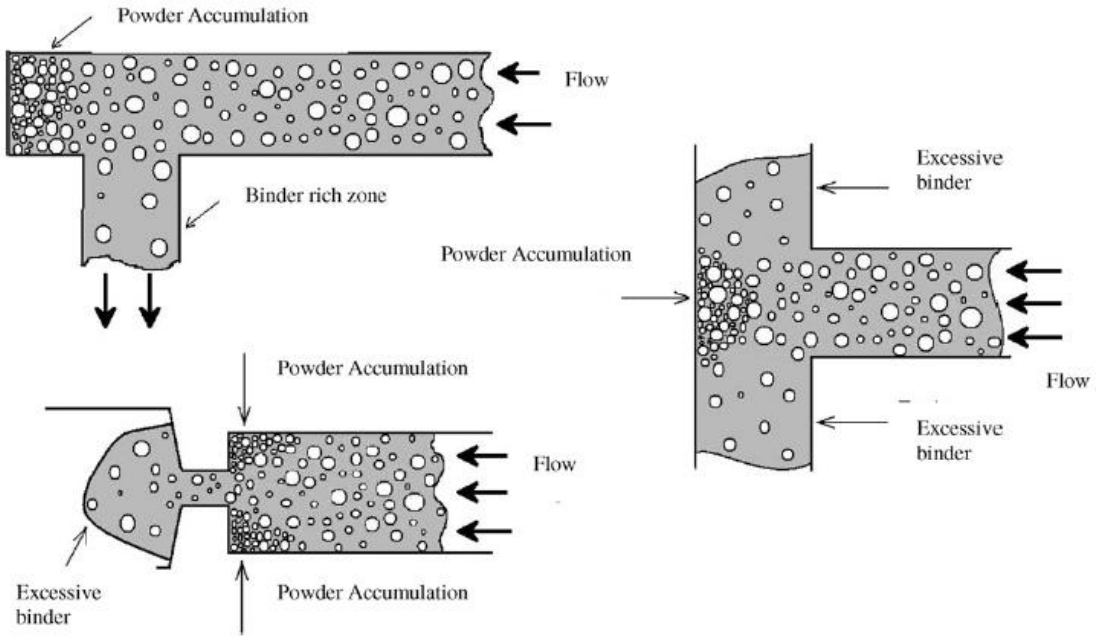

Fig. 12 – Phase separation caused by sudden geometrical changes in mold cavity (Heaney 2012)

A feedstock flow is modeled as a bulk by using of Navier Stokes equations. However, a PIM feedstock is two-phase system. Thus, the Navier Stokes equations should be formulated for each component – powder and binder, and both have to be coupled in an appropriate way as was mentioned in Section 1.1.

3.2. Practical Approach to Evaluation of Phase Separation

For experimental studies and subsequent quantification of a phase separation four types of mold designs have been used. The most widely employed moldability test for plastics measures the filling of a spiral flow channel. Moldability is expressed as a flow length of a material under certain injection

molding conditions. Injection is performed to a cold mold, which results in creating of a frozen layer on a surface between mold and cavity (Fig. 13). As a heat transfers from material to a cold mold, formation of a frozen layer is increasing, and simultaneously, a liquid feedstock area in a center of flow channel is decreasing. In comparison to plastics, PIM feedstocks have higher thermal conductivity, which leads to a faster solidification. This is the reason for higher injection rates used in PIM (German 1997, Karatas 2008).

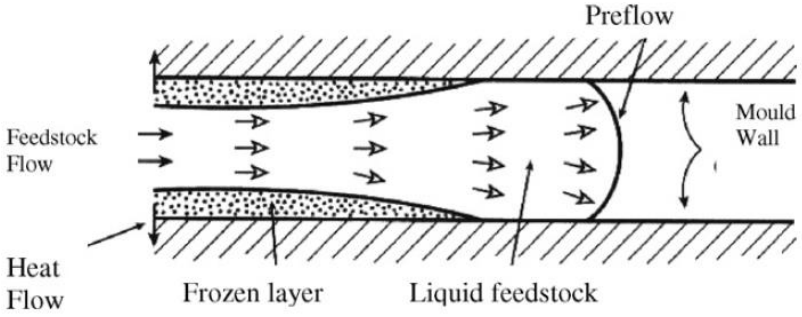

Fig. 13 – Feedstock flow along the mold canal (German 1997)

PIM feedstock in a spiral mold separates because of cold die walls, a powder rich plug is situated at a flow tip. Flow stops, when the value of pressure at the tip of a flow path decreases below the yield strength of the feedstock (German 1997, Hsu 1995).

To express moldability of PIM feedstocks, a zig-zag mold was specially designed at San Diego University back in 90´ (German 1997). Design of this mold is schematically shown in Fig. 14. Material flow is forced to change the flow direction because of side branches. During the flow, powder rich areas develop at the end of the branch, while the binder rich portion of the feedstock with substantially lower viscosity still flows down to the side branch, often before the tip is fully filled, as it is shown in Fig. 14. The zig-zag mold design often provides the basic testing of the suitability of PIM feedstocks for molding (German 1997).

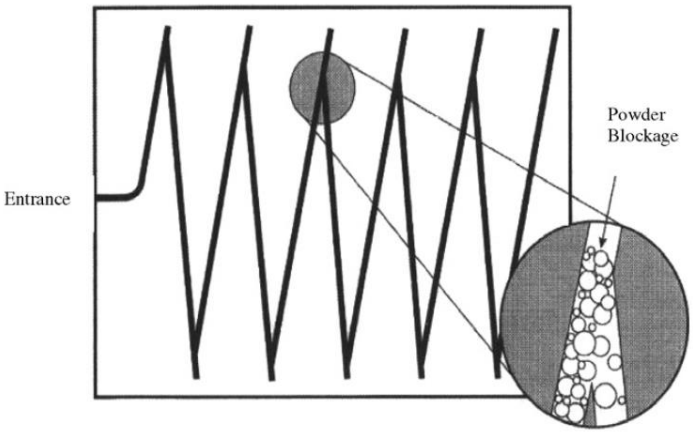

Fig.14 – Zig-zag test mold used for mouldability and separation tests (German 1997)

Furthermore, a phase separation during a flow through a square spiral mold has been studied by Jenni et al. (Jenni 2008, 2009). In this experiment differential scanning calorimetry (DSC) was used for quantifying the separation. A reference material (tungsten feedstock) with different powder loadings (30, 50, 60 vol.%) was examined and a correlation between changes of enthalpy and a binder content in these loadings was found. Afterwards, changes of a powder loading have been evaluated and quantified (Jenni 2008, Jenni 2009). The corner of the square spiral geometry has been selected as the most suitable location to determine the phase separation. First, it was divided horizontally into 3 regions/pieces. Every piece was 1 mm thick and divided to 64 small squares with 1 mm side length. Every square was examined on a DSC, and powder content was evaluated. After the measurement, the powder content 2D DSC patterns were obtained as shown in Fig. 15 (Jenni 2008).

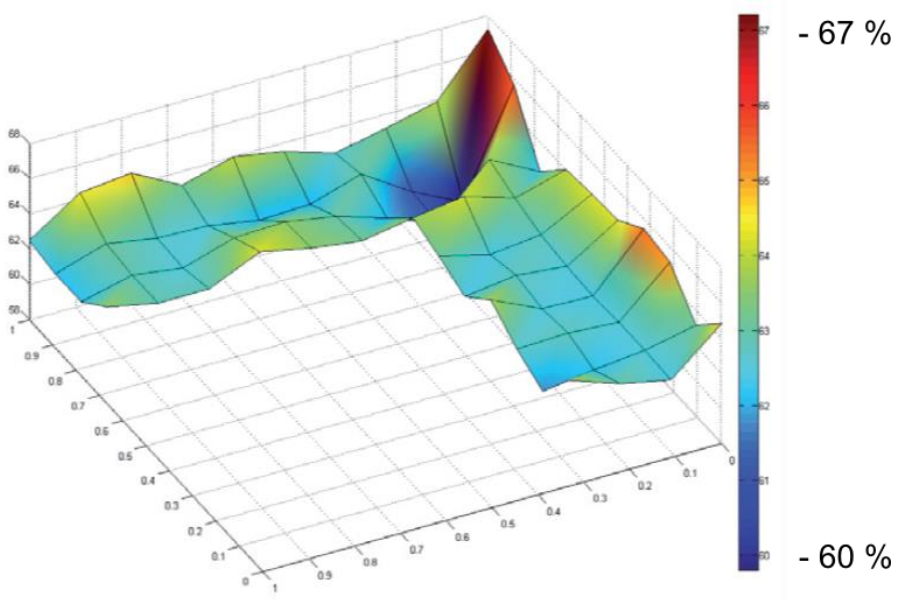

Fig. 15 – 2D DSC measurement of powder distribution in a molded sample (Jenni 2008)

The main disadvantages of this approach to determine a phase separation are inaccuracy, time consumption of sample preparation and post-process data evaluation.

Another possible method to quantify powder/binder distribution is a computer tomography, which represents a non-destructive method of a structure analysis of materials. Yang *et* al. (Yang, 2015) in his study presented an evaluation of defects inside a green body after injection molding with help of computed tomography (Fig. 16). According to his findings, pressure, temperature and injection rate are the keys to eliminate or minimize phase separation and pore formation process during injection molding. Therefore, it is necessary to understand well the conditions inside molds, especially regarding a future automatization of a PIM process.

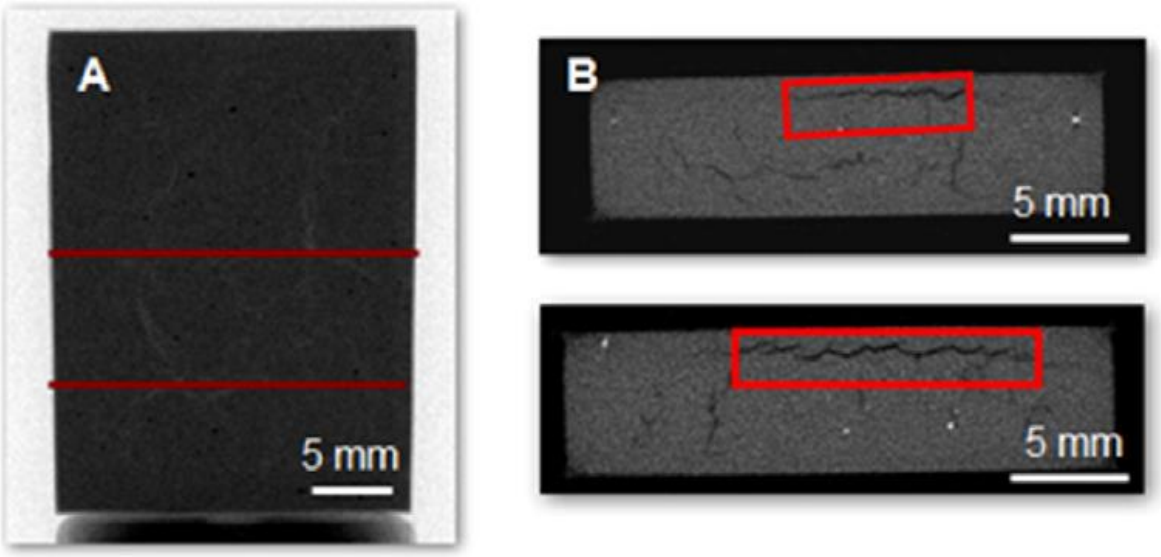

Fig. 16 – Computer tomography of PIM testing sample (a crack near surface visible on a right scan) (Yang 2015)

Recently, a new geometry to quantify phase separation (Fig. 17) has been developed at the Tomas Bata University in Zlin in cooperation with Fraunhofer IFAM, Bremen (Jiranek 2010). The testing sample consists of four sections and each section is connected with the 1 mm long gate in the section profile. The inner side length of first three sections and the outer side length of the last section is 10 mm. The mold cavity contains the inner and outer corners, the radical thickness variations, the areas with the weld lines and very thin film part, which is 0.3 mm deep (Hausnerova 2011b).

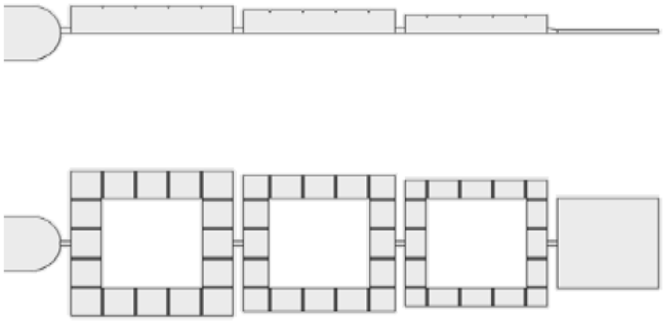

Fig. 17 - TBU/IFAM testing geometry (Hausnerova 2011b)

On this geometry, the novel evaluation method based on a scanning electron microscopy with an energy dispersive X-ray (SEM/EDX) has been proposed (Hausnerova 2013). In the methodology, the quantitative EDX mapping as the measure of separation was carried out. To convert qualitative grayscale maps into quantitative information, it was necessary to assign relative parameter, where 0 % represents purely white area and 100 % completely dark spots. Then, the

concentration EDX maps of the powder and/or the binder elements after injection molding have been analyzed mathematically to obtain the single value - so called variability parameter. The variability parameter represents the size of the powder or binder non-uniformity within the tested PIM samples. To avoid inhomogeneities from local concentration imperfections, the EDX maps have been smoothed, when each pixel was considered as an average of (5 x 5) neighboring pixels (Hausnerova 2013). The whole process of quantitative analysis is visualized in Fig. 18.

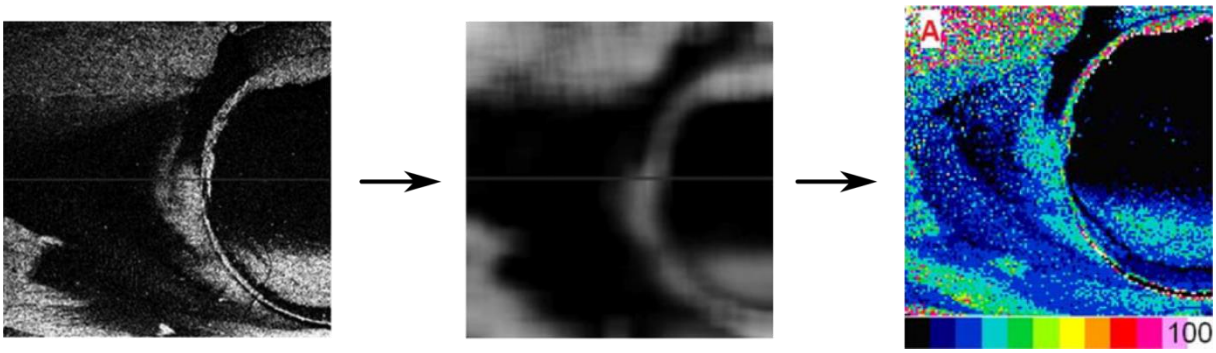

Fig. 18 - Evaluation of powder/binder content based on SEM/EDX analysis (Hausnerova 2013)

AIM OF THE WORK

The aim of this work is to propose a new view on a tool design for highly filled compounds. First task is to modify testing geometry for phase separation proposed recently by TBU and IFAM. Testing geometry intercepting main issue of injection molding of highly filled materials - phase separation - should consider findings of previous studies. Innovative approach to qualification of separation will be presented, on-line monitoring of a temperature inside mold cavity will be measured and related to simulation approach. This task has a promising commercial potential due to a current automation of production. Thanks to on-line temperature control, it will be possible to decide if part will be passed through, or grinded and re-used again in production. For this purpose, non-conventional methods of melt temperature recording will be used, specifically infrared (IR) sensors with quick response time. As additive manufacturing becomes a competitor to injection molding, the concept for production of molds from non-conventional materials for small batches will be introduced.
Main objectives of thesis are:

- material characterization for computational simulations of filling stage and Moldflow simulations of previous geometries for determination of phase separation during mold filling,
- design of a new testing mold for phase separation of highly filled PIM feedstocks with respect to previous studies,
- design of universal frame with inserts for temperature monitoring,
- correlation between Moldflow simulations of temperature profile and IR monitored temperature with the aim to determine the potential places of separation,
- experimental qualification of separation with computed tomography,
- design of testing geometry in universal frame for evaluation of weld lines of highly filled compounds, proposal of mold materials with respect to their thermal conductivity with the aim to affect mechanical properties of weld lines
- determination of tensile strength of weld lines for highly filled compounds used in conventional injection molding and PIM technology supplemented with statistical analysis.

4. METHODS

List of used molded materials:

- high-density polyethylene HD 6719 (Exxon Mobil Corp., USA) with low MFR (19 g/10min, 190 °C, 2.16 kg),
- MIM feedstock 17-4PH D 222E (PolyMIM, Germany) from X5 CrNiCuNb1 6-4 martensitic precipitation age hardenable stainless steel powder,
- WPC sawdust from processing of soft-wood, where particles with the smallest dimension above 400 μm was removed with a mesh analyser.

List of used mold materials:

- High-alloy, hot-work steel X38 CrMoV 5-1 material No. 1.2343 (Meusburger Georg GmbH & Co KG, Austria) for universal frame inserts,
- High-alloy, pre-toughened tool steel X33 CrS 16 material No. 1.2085 (Meusburger Georg GmbH & Co KG, Austria) with increased concent of chromium (16 %) and reduced thermal conductivity (18 $W.m^{-1}.k^{-1}$) for phase separation inserts,
- Unalloyed toolsteel C 45 U mat. No. 1.1730 (HASCO Hasenclever GmbH + Co. KG, Germany) for universal frame with good machinability.
- High strength aluminium alloy AlZn5Mg3Cu, EN AW 7022 (GLEICH Aluminiumwerk GmbH & Co. KG, Germany) for universal frame,
- Pure copper CW004A (ALMS spol. s r.o., Czech Republic) with 99.9 % copper content for universal frame,
- Bronze alloy CC493K (ALMS spol. s r.o., Czech Republic) for universal frame,
- high temperature resistant epoxy resin Gamod Fluid T206 (Dawex Chemical s.r.o., Czech Republic) with resistance up to 200 °C for universal frame,
- thermal filler hexagonal Boron Nitride 15/400 (3M Deutschland GmbH, Germany) with particle size distribution D_{90} up to 300 μm for universal frame,
- Mixture of acrylic monomer with photoinitiator (Stratasys, Ltd., Israel) as a VeroWhitePlus RGD 835 printing material for universal frame.

List of auxiliary materials:

- Isopropyl alcohol with 99.5 % purity (Lach-ner, s.r.o., Czech Republic)
- Silicon rubber Lukopren N1522 (Lučební závody, a.s., Czech Republic)
- Lukopren Catalyst N as a cross-link agent for two-component silicon rubber (Lučební závody, a.s., Czech Republic),

- methacrylated oligomers, monomers and photoinitiator (Formlabs Inc., USA) as a clear printing resin.

List of used equipment:

- Gas pycnometer Ultrafoam 1200e (Quantachrome GmbH, Germany) for evaluation of filler density,
- Differential scanning calorimetry DSC 1 (Mettler-Toledo s.r.o., Czech Republic) for measurement of specific heat capacity,
- C-therm TCi (C-Therm Technologies Ltd., Canada) with modified transient plane source technique for thermal conductivity measurement,
- Plasticorder PL 2000 (Brabender GmbH & Co KG) with twin screw extruder,
- High pressure capillary viscometer Rheograph 50 (GÖTTFERT Werkstoff-Prüfmaschinen GmbH, Germany) Rheometer,
- 3-axis milling machine HWT C-442 CNC (AZK, Czech Republic) for manufacturing of insert from easy to machine materials,
- 5-axis milling machine DMU 50 (DMG MORI, Germany) for steel machining of universal frame, frame inserts and testing geometry for phase separation,
- 3D printer Objet Eden 250 (Stratasys, Ltd., Israel) for mold insert with low thermal conductivity,
- 3D printer Form 2 (Formlabs Inc., USA) as a master model for creation of casted mold inserts,
- Injection molding machine Arburg 320 C (ARBURG GmbH + Co KG, Germany) for injection molding of highly filled compounds,
- Ejector type IR sensor EPSSZL (Futaba Corp., Japan) for temperature measurement in range of (60-430) °C,
- Pre-amplifier EPT-JB001 (Futaba Corp., Japan) for transformation of
- Main-amplifier EPT-001S (Futaba Corp., Japan) for IR sensor signal,
- Universal datalogger Almemo 2590 (Ahlborn Mess- und Regelungstechnik GmbH, Germany) for recording of measured data from IR sensors,
- Analogue circular thermostat (IKA-Werke GmbH & Co. KG, Germany) for water debinding bath,
- Sintering furnace MIM 3616 (Clasic, s.r.o., Czech Republic) with molybdenum heating elements,
- Desktop scanning electron microscope Phenom Pro 2000 (Thermo Fircher Scientific Inc., USA),

- Computed tomography Phoenix V|tome|x L240 (General Electric Co., USA) with acceleration voltage of 300kV/500W and micro-focus tube,
- Universal testing machine Zwick Roell 1456 (Zwick Roell Group, Germany) for tensile strength characterization.

List of softwares:

- Autodesk Moldflow Data Fitting 2018 (Autodesk, Inc., USA) for material characterization for CAE simulations,
- CATIA V5R19 (Dassault Systems) for CAD modelling, mold designing and drawings,
- Autodesk Moldflow Synergy 2016 (Autodesk, Inc., USA) for CAE simulations,
- Autodesk Netfabb Premium 2018 (Autodesk, Inc., USA) for mesh optimisation and generation,
- PreForm (Formlabs, Inc., USA) for 3D printing model preparation,
- Minitab 18 (Minitab, Ltd., United Kingdom) for statistical evaluation of sSimilarities.

For rheological measurement, a capillary rheometer with control-rate mode, where a piston speed is monitored and afterwards converted to shear rate, was used. Capillary used for measurement has flat entrance geometry and dimensions 20 mm and 1 mm for length and diameter, respectively.

To measure density of sawdust for WPC filled compounds, gas pycnometer was employed, where a sealed chamber with sawdust was pressurized with a helium gas and obtained pressure was recorder. Afterwards, pressure was transferred to an empty sealed chamber, whose volume is also known and again, pressure is recorded. According to pressure drop between the testing and the reference chamber it is possible to specify the density of the tested sample. Final density was obtained as an arithmetic mean of three measurements.

For computer simulations, Autodesk Moldflow Synergy 2016 was utilized. According to small thickness of the parts, the dual domain mesh type with at least 10 elements through the part thickness has been selected. Obtained data from material characteristics were fitted in Autodesk Moldflow Data Fitting 2018, exported as the database file and imported into the Moldflow simulation. Moldflow is using three-parameter Cross viscosity model, which intercepts viscosity at both low and high shear rate regions.

$$\eta = \frac{\eta_0(T_1)}{1+\left[\frac{\eta_0(T)}{\tau^*}\dot{\gamma}\right]^{n-1}}$$

where η is shear viscosity, $\dot{\gamma}$ is shear rate, n is the non-Newtonian index, T is the temperature and τ^* is shear stress at the transition between first Newtonian plateau and shear thinning region. If zero shear rate viscosity η_0 is calculated according to Williams-Landel-Ferry equation, Cross model is turned to WLF-Cross model, which is widely used in numerical simulations of injection molding. In this case, WLF zero shear viscosity reflects the temperature and pressure effect more precisely:

$$\eta_0 = D_1 \exp\left\{\frac{-A\left[T-\left(D_2+D_3 p\right)\right]}{A_2+T-D_2}\right\}$$

where A_1, A_2 and D_1, D_2, D_3 are material parameters obtained from data fitting.

First, simulations were performed to verify previous findings of Jenni (2009) and Hausnerova (2013) in the area of phase separation, second, simulation of temperature development in the particular selected points of the new proposed mold design to intercept separation.

Tools were designed for Arburg 320C, which is suitable for highly filled materials causing an abrasive wear on mold and molding equipment with clamping force of 70 tones and D = 20 mm in case of screw from injection unit.

Machining of the universal frame and all inserts for testing was done on 3-axis and 5-axis milling machines with SECO tools with suitable geometry for currently machined material.

3D printing of mold insert was done with the help of Objet Eden 250 with 25 μm layer thickness, and master model for casting of silicone mold and, subsequently mold insert from epoxy resin, was done on Formlabs Form 2 3D printer with 50 μm layer thickness.

For mechanical testing, Zwick Roell 1456 machine was used. Due to expectation of high tensile properties, samples were clamped into pneumatic grippers. Testing speed profile was divided into two regions according to ČSN EN ISO 6892-1:

- evaluation of Young modulus up to 0.2 % of relative elongation, where speed was set to 5 mm/min,
- determination of ultimate strength under speed of 20 mm/min.

Testing specimen was designed with respect to EN ISO 2740:2009 - Sintered Metal Materials, Excluding Hardmetals - Tensile Test Pieces. According to Hausnerova *et* al. (Hausnerova, 2014b) one discrepant dimension has been received from MPIF standard - Preparing and Evaluating Metal Injection Molded (MIM) Sintered /Heat Treated Tension Test Specimens. Fundamental dimensions are depicted in Fig. 19.

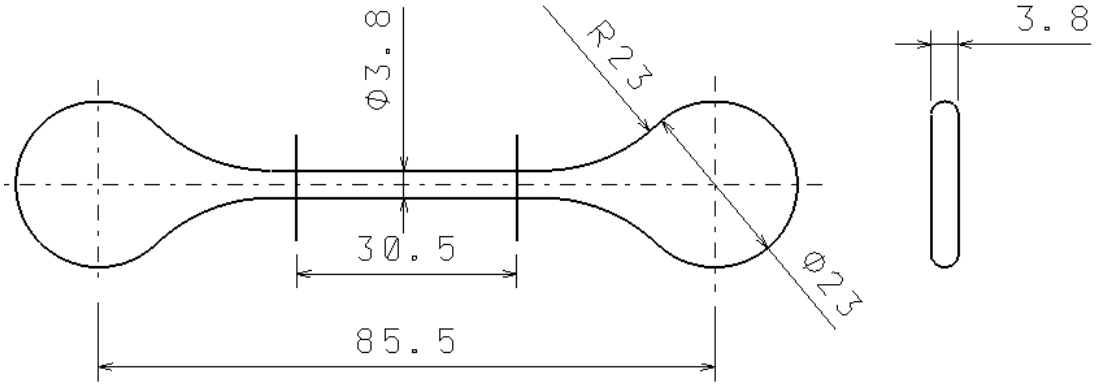

Fig. 19 - Dimensions of Tensile Test Specimens

For determination of an outlier value, Grubbs test was selected. Grubbs test is performed as hypothesis test, which is defined as:
H_0: in the data sample is no outlier,
H_a: the maximum or minimum value in the data sample is an outlier
at a significance level of $\alpha = 5$ %

To test the equal variances, Levene test was employed with the following hypotheses:
H_0: all variances are equal,
H_a: not all variances are equal
at significance level of $\alpha = 5\%$

Analysis of variance tests the hypothesis that the means of sample populations are equal. Hypothesis was compiled as:
H_0: all population means are equal,
H_a: at least one population mean is different
at significance level of $\alpha = 5$ %

Cluster analysis is focused on an establishment of clusters, where cases within the cluster are more similar to each other than are cases in next clusters. Jain *et* al. (Jain, 1999) defined several clustering methods, and the hierarchical clustering method has been selected for this Thesis.

Rearranging into the groups was done with Ward method, where the distance between two clusters is the sum of squared deviations from points to centroids

The ordinary method of least squares is a statistical method used in linear regression. In linear and polynomial regression.

5 RESULTS AND DISCUSSION

5.1. Material characterization

The highly filled compounds (WPC and PIM) were characterized with the respect to flow simulations. Wood sawdust as a waste material was separated from large fraction above 400 μm with mesh analyzer and afterwards density was characterized with gas pycnometer Ultrafoam 1200e in helium. As a result, density of 0.196 g/cm^3 was obtained. To prepare highly-filled WPC feedstock, first HDPE polymer matrix with sawdust was mixed in ratio 50:50 vol.%. Subsequently, the mixture was further homogenized by extrusion using a twin screw extruder (nozzle temperature: 200 °C, Zone 2: 190 °C, Zone 1: 180 °C, screw rotations: 50 rpm) and granulated. Second highly filled testing material is commercially available MIM feedstock PolyMIM 17-4PH D 222E.

5.1.1. Thermal Conductivity

Thermal conductivity is necessary for determination of cooling rates. Insert materials with the lower thermal conductivity than molded material (17-4PH) were selected with the purpose to maximize the packing phase in molding cycle. Thermal conductivity was measured with C-therm device, where modified transient plane source technique is used. A known current is applied to a sensor's heating element providing a small amount of heat. The current applied to the coil results in the temperature elevation at the interface between the sample and the sensor, subsequently the voltage drop is inducted. Testing samples were machined (in case of copper, aluminium, steel 1.2085, bronze), casted (epoxy resin, epoxy resin + 35vol.% hexagonal boron nitride - hBN), pressed (PIM 17-4PH, WPC) or 3D printed. Testing sample dimensions were 20 mm in diameter and 12 mm/22 mm in height for thermal conductivity bellow/above 90 W.m^{-1}.k^{-1}, respectively.

Table 1 - Thermal conductivity for tested feedstocks and insert materials

Material	$\bar{x}$	s	v
	[W.m^{-1}.k^{-1}]		[%]
Copper	383.941	14.860	3.870
Aluminum	154.024	2.164	1.405
Bronze	64.198	1.504	2.343
Steel 1.2085	17.276	0.311	1.800
Epoxy resin + 35% hBN	0.992	0.015	1.541
Epoxy resin	0.390	0.007	1.700
3D printed	0.204	0.007	3.656
PIM 17-4PH	4.155	0.145	3.483
WPC	0.205	0.005	2.600

5.1.2. Rheology

Viscosity curves were obtained for three temperatures - 180, 190, and 200 °C. The data is depicted in Table 2.

Table 2 – Viscosity curves for 17-4PH and three different temperatures

Temperature	Shear rate	Shear stress	Viscosity
[°C]	[s^{-1}]	[Pa]	[Pa.s]
180	35	76903	2197
	60	94641	1577
	100	115500	1155
	170	145565	856
	290	184343	635
	490	233995	477
	830	297518	358
	1410	371660	263
	2400	491193	204
	4000	657984	164
190	35	76026	2172
	60	92999	1549
	100	112516	1125
	170	137518	808
	290	172191	593
	490	217313	443
	830	271990	327
	1410	340271	24
	2400	436568	181
	4000	561143	140
200	35	75150	2151
	60	91356	1528
	100	109532	108
	170	129470	765
	290	160040	550
	490	200630	412
	830	246463	281
	1410	308883	219
	2400	381943	169
	4000	464301	121

5.1.3. Specific Heat Capacity

For deceleration reason of cooling rate due to phase transformation, a specific heat capacity c_p of molding materials was measured. The data is crucial for simulation of temperature profiles in pre-selected areas, and finding of regression function. Specific heat capacities were evaluated from DSC measurement with 90 °C/min cooling rate.

Table 3 - Specific heat capacity for selected temperatures for 17-4PH

Temperature [°C]	**30**	**50**	**55**	**60**	**65**	**70**
c_p **[J/g^{-1}.°C]**	0.435	0.601	0.772	1.083	0.721	0.611
Temperature [°C]	80	90	100	110	120	130
c_p **[J/g^{-1}.°C]**	0.623	0.537	0.542	0.463	0.421	0.411

5.1.3. Sample Preparation

For injection molding, Arburg 320C suitable for highly filled materials, was used. Processing conditions for the phase separation testing mold and injection molding of MIM feedstock PolyMIM 17-4PH D222E are described in Table 4. Temperature profile was set with respect to material datasheet recommendations, and pressure was adjusted to fullfill the injection mold cavity.

Table 4 - Parameters of injection molding for 17-4PH feedstock for phase separation

Separation Mold	Nozzle	Zone5	Zone 4	Zone 3	Zone 2	Zone 1
Barrel Temperature [°C]	180	176	172	168	164	160
Mold Temperature [°C]	65					
Injection Pressure [bar]	2200					
Injection Speed [mm/s]	100					
Switch-over method	piston distance					
Switch-over value	95% of injected volume					
Holding Pressure 1 [bar]	2000					
Duration 1 [s]	0.5					
Holding Pressure 2 [bar]	2200					
Duration 2 [s]	3.0					
Holding Pressure 3 [bar]	400					
Duration 3 [s]	0.5					
Cooling Time [s]	30					

In case of testing of the influence of the thermal conductivity of mold inserts on the mechanical properties, namely the tensile strength, processing conditions are

listed in Table 5 for PolyMIM 17-4PH feedstock and in Table 6 for WPC compound. Injection pressure was determined as requested pressure to full-fill the insert from copper with the highest pressure drop due to rapid solidification, and for all next inserts was the same to keep comparability of the results.

Table 5 - Parameters of injection molding for 17-4PH for insert testing

17-4PH Insert Mold	Nozzle	Zone 5	Zone 4	Zone 3	Zone 2	Zone 1
Barrel Temperature [°C]	180	176	172	168	164	160
Mold Temperature [°C]	45					
Injection Pressure [bar]	1500					
Injection Speed [mm/s]	50					
Switch-over method	piston distance					
Switch-over value	95% of injected volume					
Holding Pressure 1 [bar]	1400					
Duration 1 [s]	0.5					
Holding Pressure 2 [bar]	1300					
Duration 2 [s]	3 (metal inserts), 10 (polymeric inserts)					
Holding Pressure 3 [bar]	200					
Duration 3 [s]	0.5					
Cooling Time [s]	120					

Table 6 - Parameters of injection molding for WPC for insert testing

WPC Insert Mold	Nozzle	Zone 5	Zone 4	Zone 3	Zone 2	Zone 1
Barrel Temperature [°C]	200	195	190	185	180	170
Mold Temperature [°C]	45					
Injection Pressure [bar]	1700					
Injection Speed [mm/s]	50					
Switch-over method	piston distance					
Switch-over value	95% of injected volume					
Holding Pressure 1 [bar]	1550					
Duration 1 [s]	0.5					
Holding Pressure 2 [bar]	1400					
Duration 2 [s]	3 (metal inserts), 10 (polymeric inserts)					
Holding Pressure 3 [bar]	200					
Duration 3 [s]	0.5					
Cooling Time [s]	120					

Requested holding pressure is calculated as 80 % of maximum filling pressure, and duration of this phase should last up to the solidification of the smallest cross-section of flow domain - gate. Therefore, if thermal conductivity of inserts was below feedstock conductivity (polymeric inserts), duration of packing was set to 10 s (and vice versa for metal inserts with 3 s duration).

For debinding of PolyMIM 17-4PH, a two step binder removal method was used. In first step, green parts were soaked in distilled water with 2 vol.% of corrosion inhibitor (Inhibitor 4000, Zschimmer & Schwarz). Water soluble binder was dissolved for 18 h at temperature 60 °C. After first stage of debinding, the green parts were dried in oven at 80 °C for 6 hours.

After drying, parts were placed on sintering plates made of Al_2O_3 due to higher sintering temperature of ceramic and no bonding between parts and sintering plate. Pure nitrogen at the pressure of 300 Pa was used as a sintering atmosphere. Sintering cycle was set with the respect to the material datasheet.

5.2. Mold Concept for Universal Frame

Universal mold frame for phase separation test insert and inserts with different thermal conductivity was designed. This frame is characterized by versatility, where core and cavity plates are in a form of inserts, and therefore, one frame is used for both issues. The tool consists of standards used in toolmaking, and cavities in plates are tailored to research needs. Therefore, sprue bushing on universal frame is made from 1.2826 tool steel hardened up to 54 HRC. All other parts are in no-contact with highly filled polymeric melt, thus for plates unalloyed tool steel 1.1730 without hardening was used due to its excellent machinability.

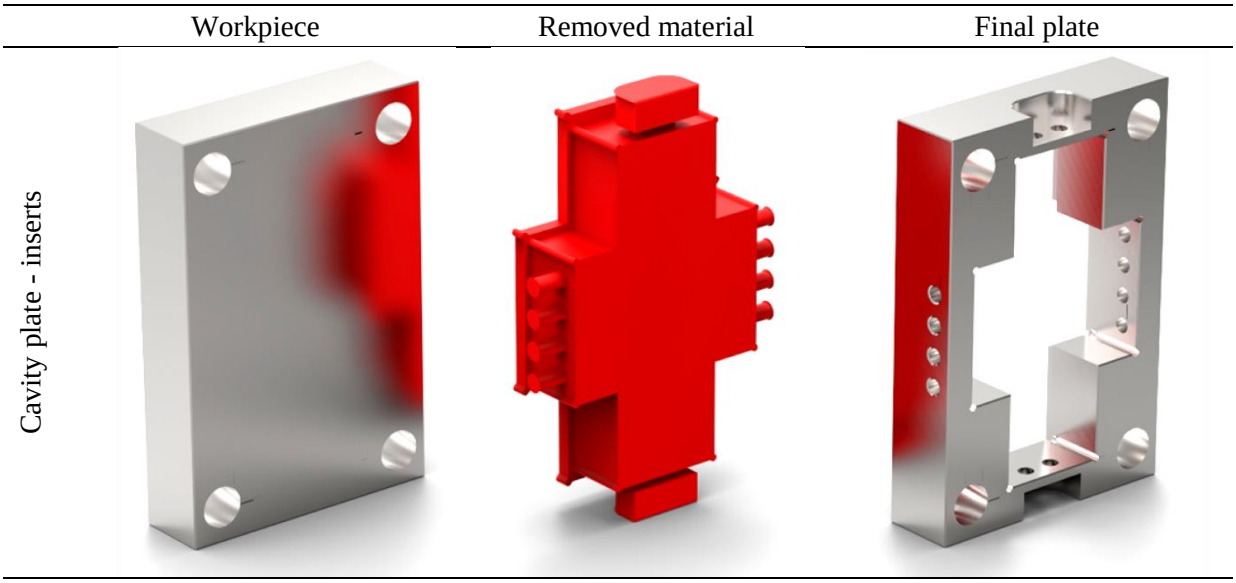

Fig 20 – Comparison of standard plate (left), removed material (middle) and final plate (right) for Cavity plate

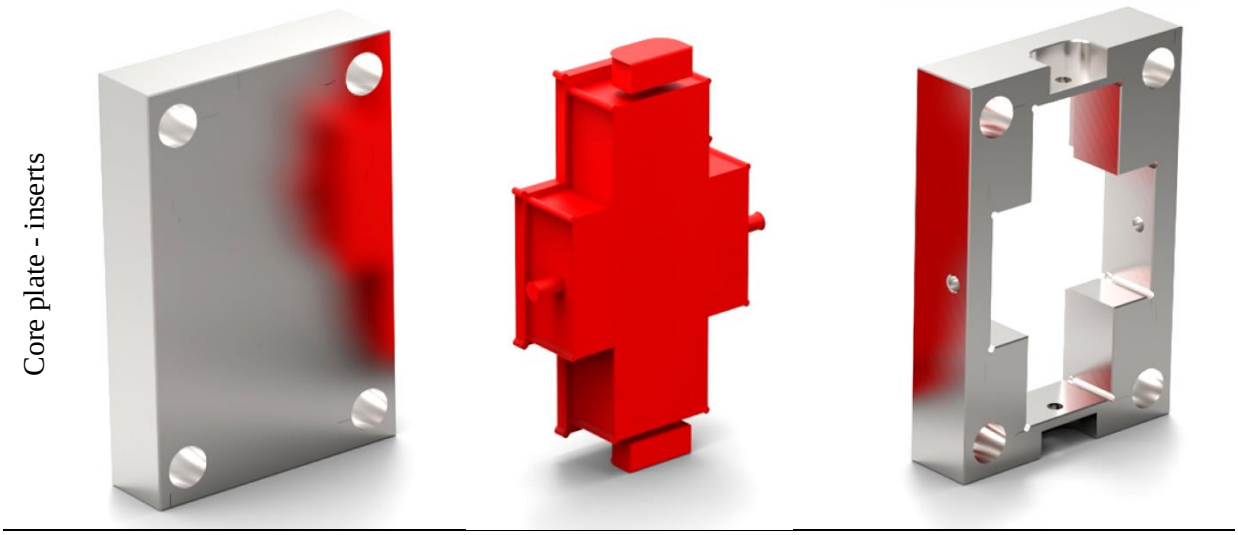

Fig 21 - Comparison of standard plate (left), removed material (middle) and final plate for Core plate

Design of suitable inserts for universal frame for phase separation and weld line study is proposed and drawings are attached to the work.

5.3. Mold Concept and Verifications for Phase Separation

Based on the previous studies in the field of phase separation during flow of filled compounds (Hausnerova, 2011, German, 1997, Jenni, 2008, Jiranek, 2010), a new mold design is proposed. The testing sample should respect features, which are supporting segregation of powder from binder. Molds for highly filled compounds as those used in powder injection molding obviously contain not only one feature supporting phase separation, but a combination of several elements: dead branches, sudden cross-section profiles changes, outer corners, weld lines. Following this consideration, it is necessary to ask the question, how the combination of critical features will affect an overall phase segregation. Previous findings of phase separation were compared to Moldflow simulations for better understanding to design approach.

Square spiral has been meshed by more than 200,000 tetrahedron elements with 1 mm edge length. In region of interest the 3D mesh was densified and element edge length was decreased to 0.2 mm. Simulated material was 17-4PH feedstock. Its rheological properties, specific heat capacity and thermal conductivity were, with support of Autodesk Moldflow Data Fitting, fitted to constants used in Cross model, where temperature-induced physical changes are predicted with Williams-Landel-Ferry equation (WLF). Both models were used in afterwards Moldflow simulation, where filling of current testing molds were simulated. Temperatures of melt and mold have been set on 180 °C and 60 °C, respectively. Filling stage was controlled by flow rate of 20 cm^3/s and evaluation was focused on third corner of testing geometry as was done by Jenni (Jenni, 2008) in Fig. 23. From results of Jenni's measurement of phase separation with

X-ray tomography (Fig. 23, right) it is evident that differences in absorbed X-ray, and therefore different density of final structure trends to copy shear rate distribution (Fig. 23, middle).

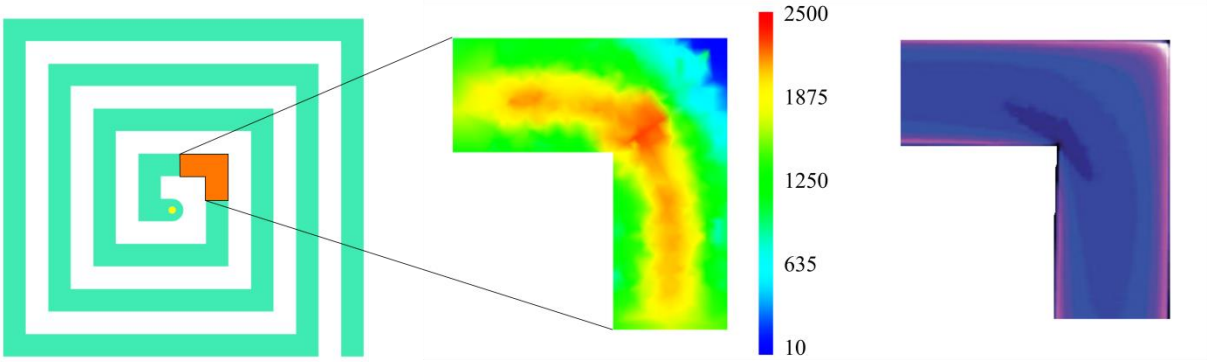

Fig. 23 – Maximum shear rate during filling stage (middle) for Jenni's geometry testing mold with reported phase separation after injection displayed by CT, (right) for 20 cm^3/s flow rate

First, simulation of injection molding stage of testing mold designed in cooperation between TBU and IFAM was performed. Material for simulation was 17-4PH feedstocks as in previous case with the same processing conditions. 3D model was discretized with 266,000 tetrahedron elements with 0.5 mm edge length. From the simulation (Fig. 24, left) it is evident that the deviation of shearing intensity from the bulk shear rate represents the area, where the phase separation occurred in the real sample, see SEM micrograph in Fig. 24, right.

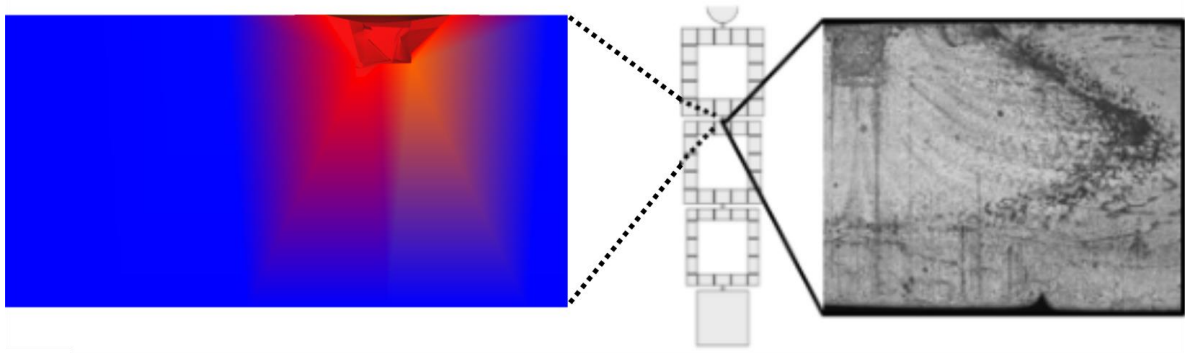

Fig. 24 – Maximum shear rate during filling stage (left) for TBU/IFAM testing mold with reported phase separation after injection displayed on SEM (right) for 20 cm^3/s flow rate

Pursuant to findings of this analysis, a new mold design has been developed with number of supporting elements for phase separation. The mold concept is based on dead branches (Fig. 25) as proposed also by German *et* al. (German, 1997), where phase separation occurs due to different momentums of powder and binder. Further, the proposed design allows to study properties of weld lines due to obstacles incorporated in testing geometry (Fig. 25).

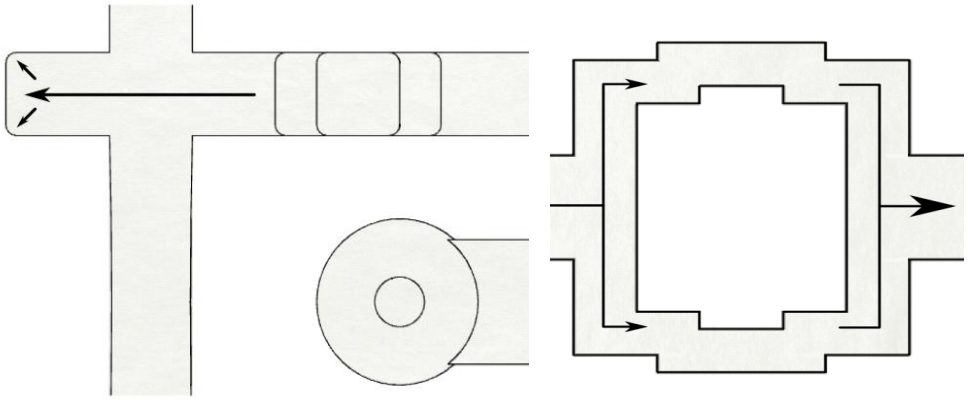

Fig. 25 - Incorporation of dead branches (left) and obstacles to forma weld line (right) into new testing mold design

Following the finding of Jenni *et* al. (Jenni, 2009) and Hausnerova *et* al. (Hausnerova, 2013), the phase separation occurs in the areas along the sharp corners and the cross section changes, respectively. Therefore, the proposed design consists of combination of both supporting elements and design of this feature is shown in Fig. 26.

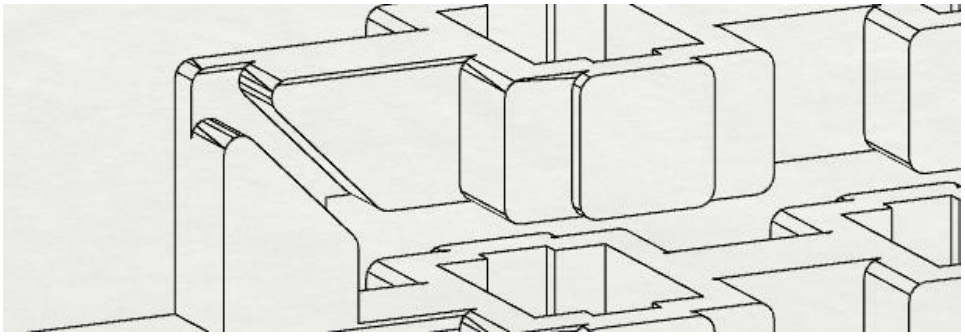

Fig. 26 - Sharp corner at sudden cross-section change in new testing mold design

Further, the proposed design allows to study properties of weld lines due to obstacles incorporated in testing geometry (Fig. 25 right). These obstacles create multiple weld lines, which mechanical properties will be investigated, and effect of multiple weld line will be evaluated (Fig. 27).

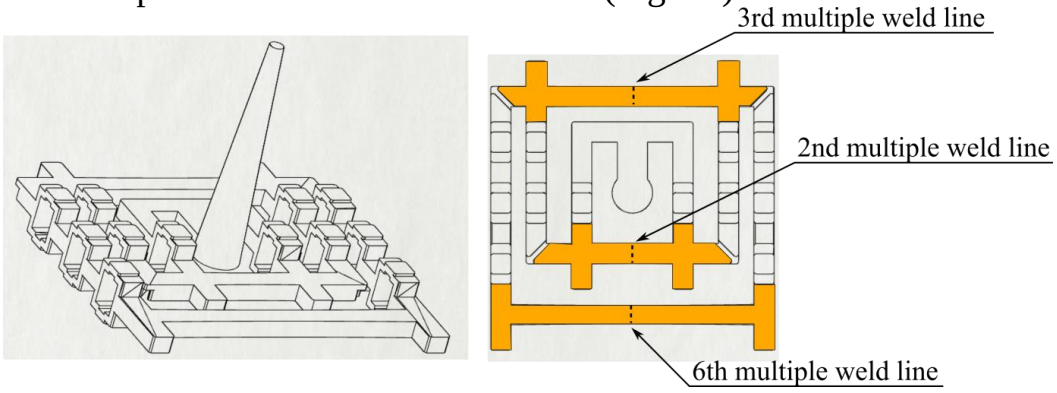

Fig. 27 - Multiple weld lines integrated in new testing mold design

The final geometry of new testing mold concept was registered as the utility model with the registration number CZ 2014-30495 U1. The geometry was designed using Moldflow simulation SW with the same processing conditions and material as in previous verifications (17-4PH, Table 4). Generated 3D mesh consists from 400,000 tetrahedron elements with 0.8 mm edge length. The result of shear rate development is depicted in Fig 28, where it is evident that the element with the highest potential to phase separation are the sharp corners at the sudden cross-section changes.

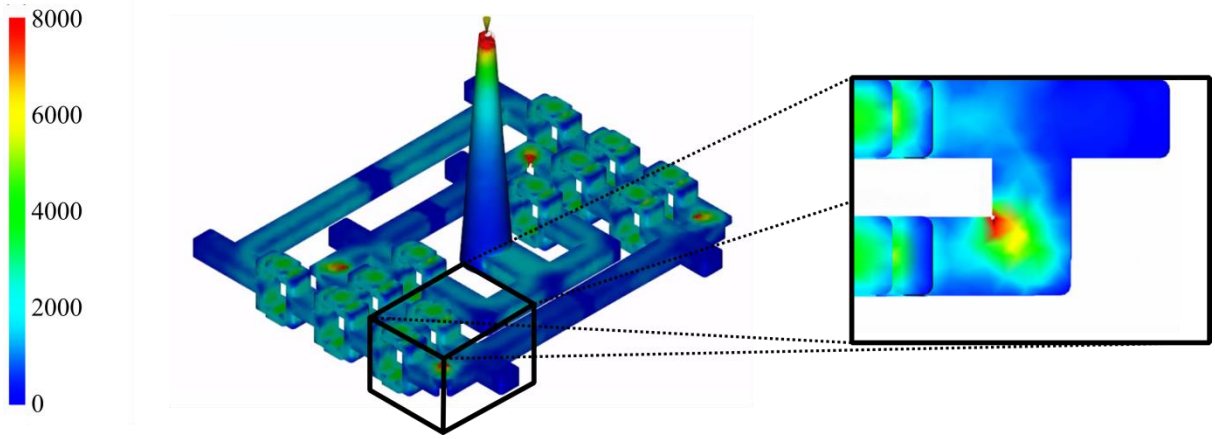

Fig. 28 - Simulation of shear rates (s^{-1}) of new testing mold for 17-4PH feedstock and conditions described in Table 4

According to moldability of the designed part, small changes needed to be done, Fig.29. To ensure the part position on the moving side of the mold after opening, it was necessary to add a fillet on the side, which is in contact with the stationary plate. There are no undercuts on the part and the right position during opening of the mold is supported with no-bevel on the side molded in the moving plate. This solution could lead to a higher ejection force, and consequently, deformation or damage of molded parts. To minimize the stress concentration in the investigated area (the corner with the sudden cross-section change, Fig. 26), the outer corner was rounded with R=1.5 mm. Number of obstacles was reduced due to the absence of formation of a simple weld line. Shape of obstacles was changed from rectangular to cylindrical.

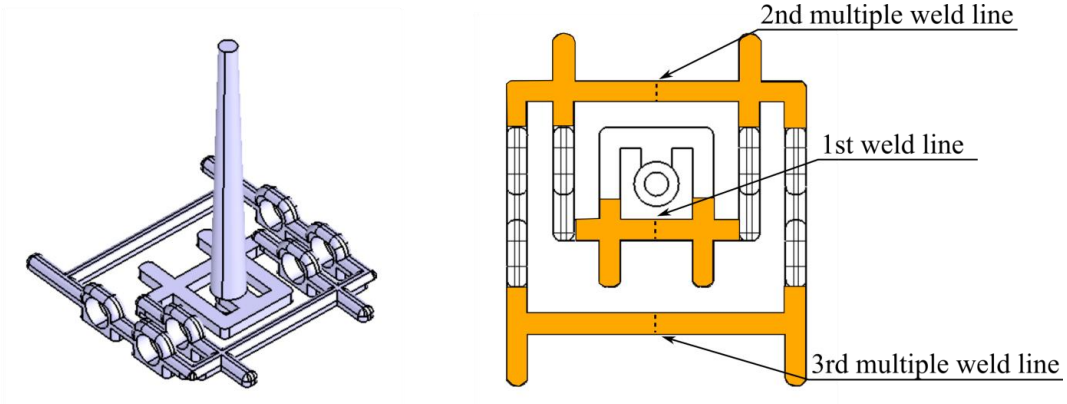

Fig. 29 - Modified testing mold to enhance moldability

Afterward, the flow in the modified testing geometry was simulated again. Model was discretized with a tetrahedron mesh. Due to the presence of the rounded elements, which cannot be neglected, the edge length of the element was set to 0.25 mm, and the number of elements exceed 1,150,000.

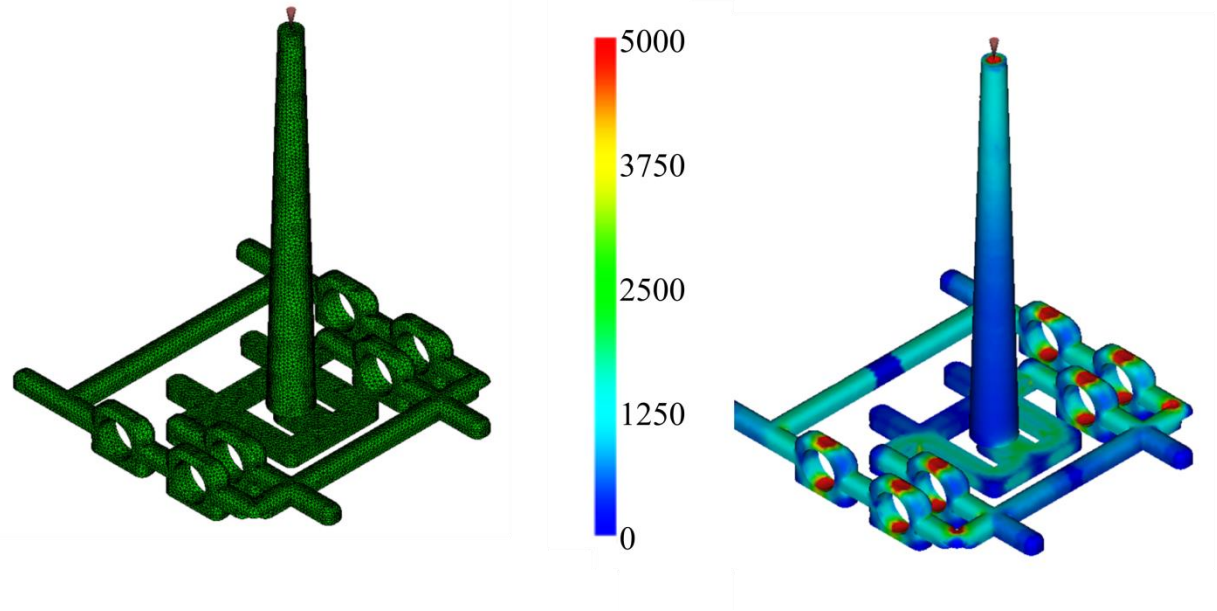

Fig. 30 - Simulation of shear rate (s^{-1}) of final testing mold for 17-4PH feedstock at conditions described in Table 4

During the simulation, the positions of 6 infrared (IR) sensors was determined as shown in the Fig. 31 displaying the temperature distribution in the mold.

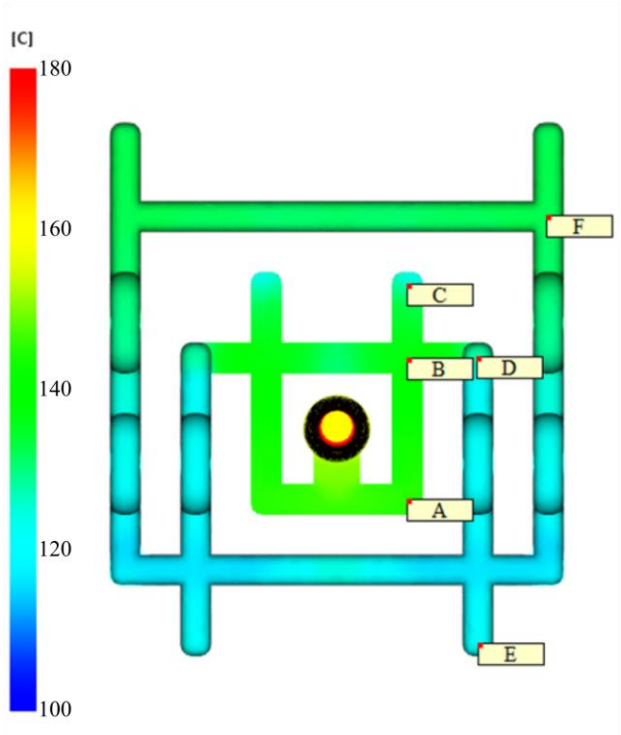

Fig. 31 - Positions of infrared sensors (A-F) determined from the simulation.

Sensor in position A is used to monitor the initial value of the melt temperature after temperature change due to the cold runner system. B sensor is located in the place, where the flow is split into three: first flow forms the first weld line, second reaches the dead branch, where C sensor is located, and third continues mold filling. D sensor depicts the temperature change due to the sharp corner, and the distance between B-C sensors and B-D sensors is kept the same. E sensor belongs to the second dead branch, and the melt reaches this area after passing through the first obstacle, where the cross-section undergoes continuous change. The last sensor F is located close to the end of the filling, and between D-F material passes through 3 obstacles with the continuous cross-section changes, and along the sharp edge with the sudden change in the cross-section profile.

From the simulation, the temperature development (Fig. 32) in these six areas was recorded.

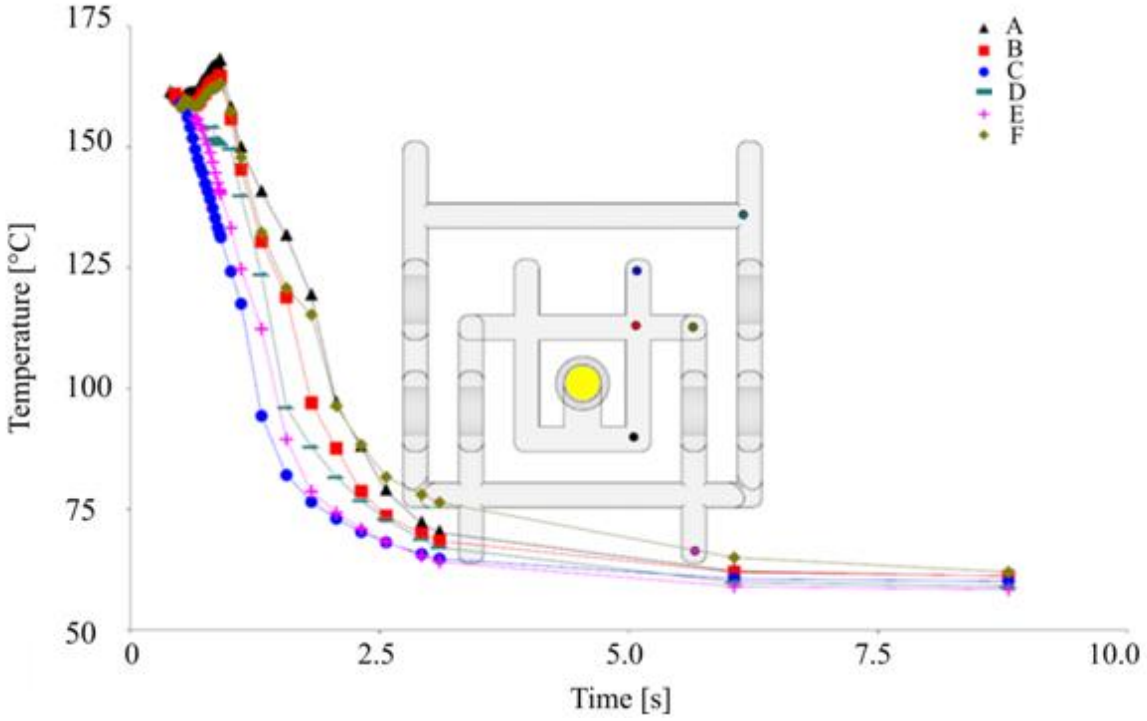

Fig. 32 – Simulation of temperature development at IR-sensor positions

After the construction of the testing mold, the real observations in preselected areas with IR sensors will be done, and results will be compared to verify the simulation results.

5.4 Results for Phase Separation Mold

Ejector-type IR sensor with diameter D = 4 mm (IT6) and length L = 160 mm (IT6) was clamped into ejector plate instead of cylindrical ejector with the same diameter. Clamped IR sensor in ejector plate was connected to pre-amplifier, which converts an optical signal to an analogue electrical signal, which passes

through main amplifier, where 100 °C represents 1 V on output. Data from main amplifier is recorded with data logger in 100 ms sampling frequency and stored to PC. The scheme of the temperature monitoring is illustrated in Fig. 33. Orange color highlights the schematic view of the temperature monitoring experiment. To ensure moldability of testing geometry, test arrangement was extended for pneumatic system (represented with blue color) that ensures formation moving of core pins to formation of obstacles presented in Fig. 25 (right).

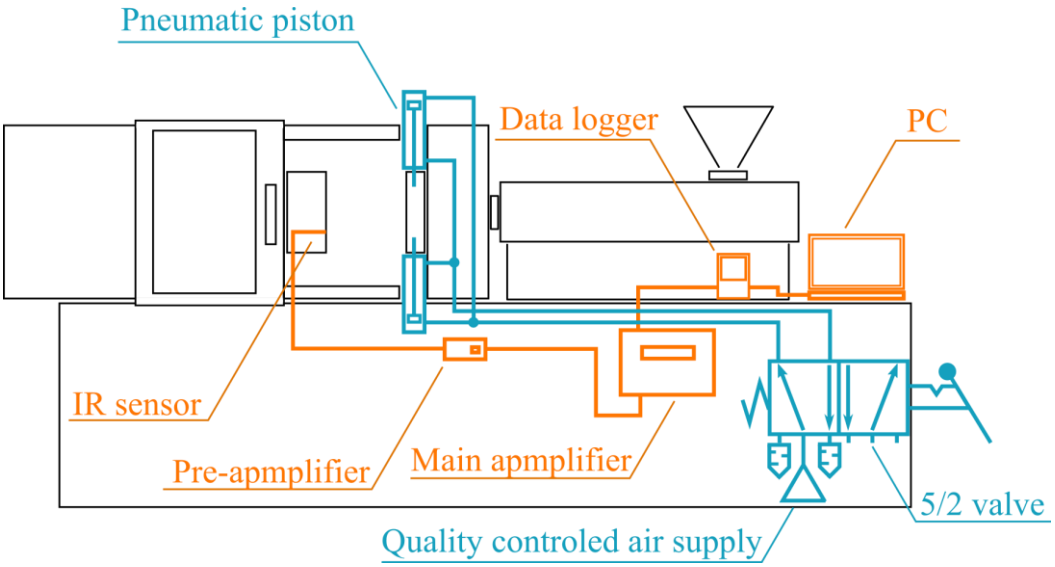

Fig. 33 – Test arrangement of temperature monitoring

Data obtained from IR sensors was aligned according to maximum temperature. Due to the fact that the obtained data are discrete values (Fig. 34), all measurements were repeated 12 times to minimize inaccurate peak values.

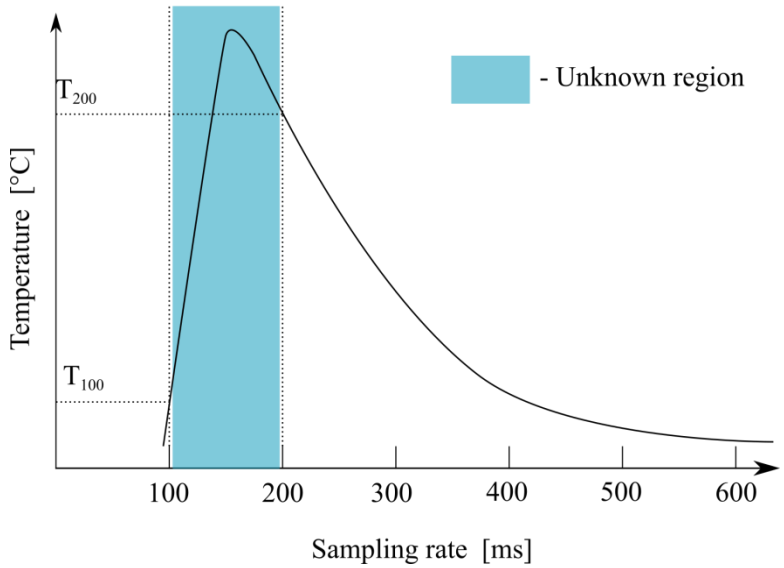

Fig. 34 - The weakest point of IR measurement

Data from all sensors was investigated with a cluster analysis to find similarities between positions; the results are shown in Fig. 35.

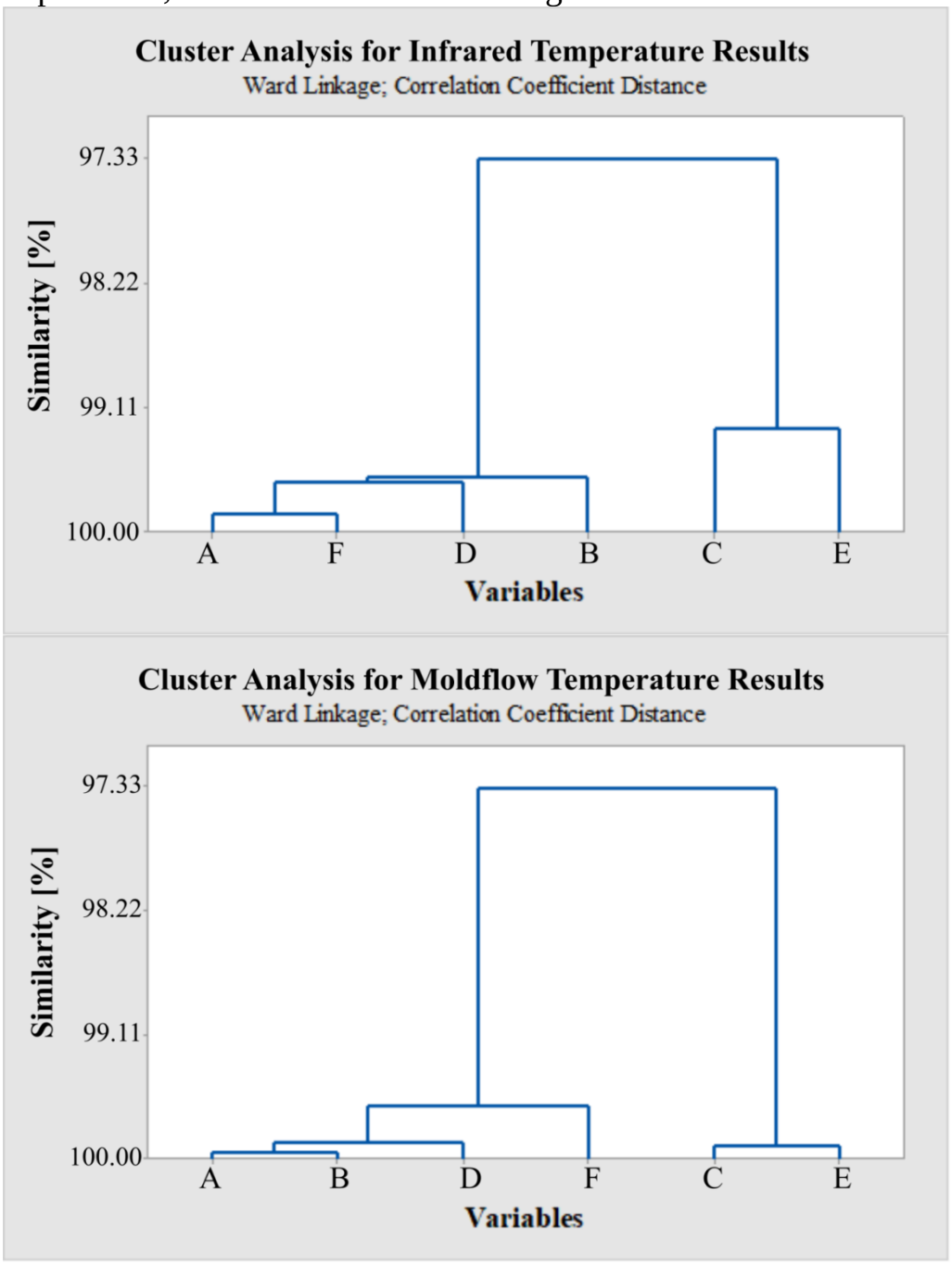

Fig. 35 – Cluster analysis of data from IR sensors (upper) and Moldflow simulation (lower) with Ward linkage method

From the cluster analysis (Fig. 35) it is evident that the temperature development for positions C and E differ in comparison to A, B, D, F positions due to their location in dead branches. While on the sensors A, B, D, F sample core of test specimen is used as a transport channel to fulfill the mold, positions of C and E sensors are in the areas, where the solidification takes place (material is not moving).

To find the best regression model, three types of regression function were used: linear, quadratic and cubic;

Table 7 - Overall results for regression functions for all IR sensors

	Linear regression	Quadratic regression	Cubic regression
IR A	95.99 %	99.55 %	99.54 %
IR B	90.71 %	98.49 %	98.48 %
IR C	88.23 %	99.53 %	99.57 %
IR D	95.67 %	98.13 %	98.11 %
IR E	82.16 %	97.00 %	99.60 %
IR F	95.31 %	99.57 %	99.59 %

Adjusted regression coefficient R^2 representing the proximity of the data to the fitted regression curve was divided into three sections, Table 7. Results of R^2 between (98-100) % was considered as a good fit (green color), (98-96) % represents sufficient fitting (orange color) and the R^2 value below 96 % is considered as insufficient model fit (red color). The linear regression model is not suitable for determination of temperature development. Quadratic and cubic model are eligible. Since the model should be simple, less parameter - quadratic model was used further.

The same philosophy was applied on data from Moldflow (MF) analysis (Table 8.)

Table 8 - Overall results for regression functions for all MF sensors

	Linear regression	Quadratic regression	Cubic regression
IR A	97.57 %	98.04 %	99.80 %
IR B	96.57 %	98.10 %	99.61 %
IR C	87.03 %	99.33 %	99.30 %
IR D	95.32 %	97.34 %	98.67 %
IR E	97.57 %	98.04 %	99.80 %
IR F	96.57 %	98.10 %	99.61 %

The same methodic for evaluation of regression functions of Moldflow results as for IR sensors is adopted. From Table 8 is noticeable that linear regression is not suitable for our purpose and quadratic regression is sufficiently precise with small number of parameters.

5.4.2 Experimental Qualification of Separation

Fifth corner of test specimen for phase separation has been inspected in detail. The reason for this location is that it contains sharp edges, rapid variations in a cross section and flow direction, and according to simulations, this feature supports phase separation (Section 5.3).

Furthermore, a higher melt temperature was measured at sensor location F, than in case of previous sensor location (E). Therefore, the potential of the separation due to increased dissipation heat (initialized by shear rate) is evident.

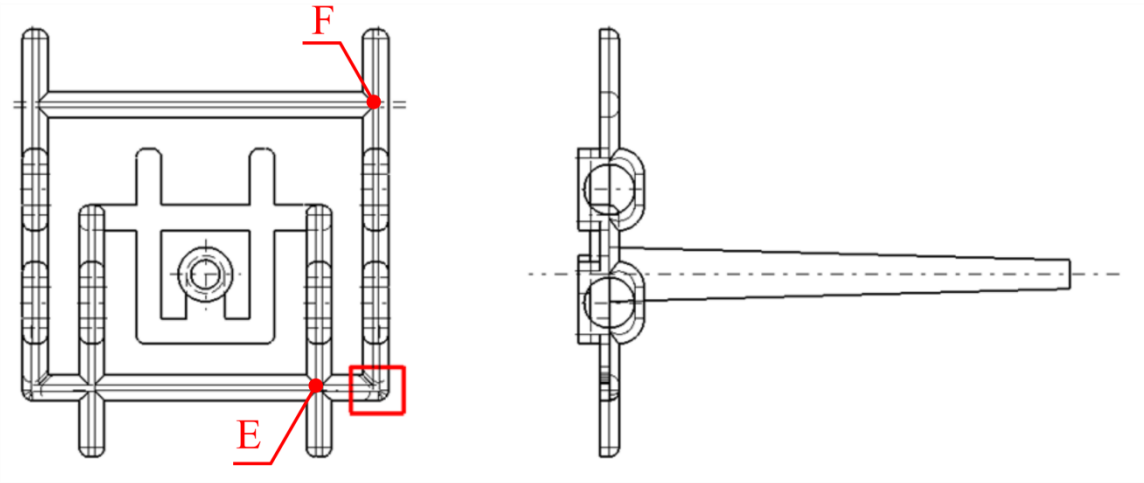

Fig. 36 - Position of fifth corner selected for detailed inspection

From SEM, the powder/binder separation is evident on the surface (Fig. 37) what brings the question if the same trend is inside the testing specimen. Therefore, a computed tomography (CT) was employed, Fig. 38.

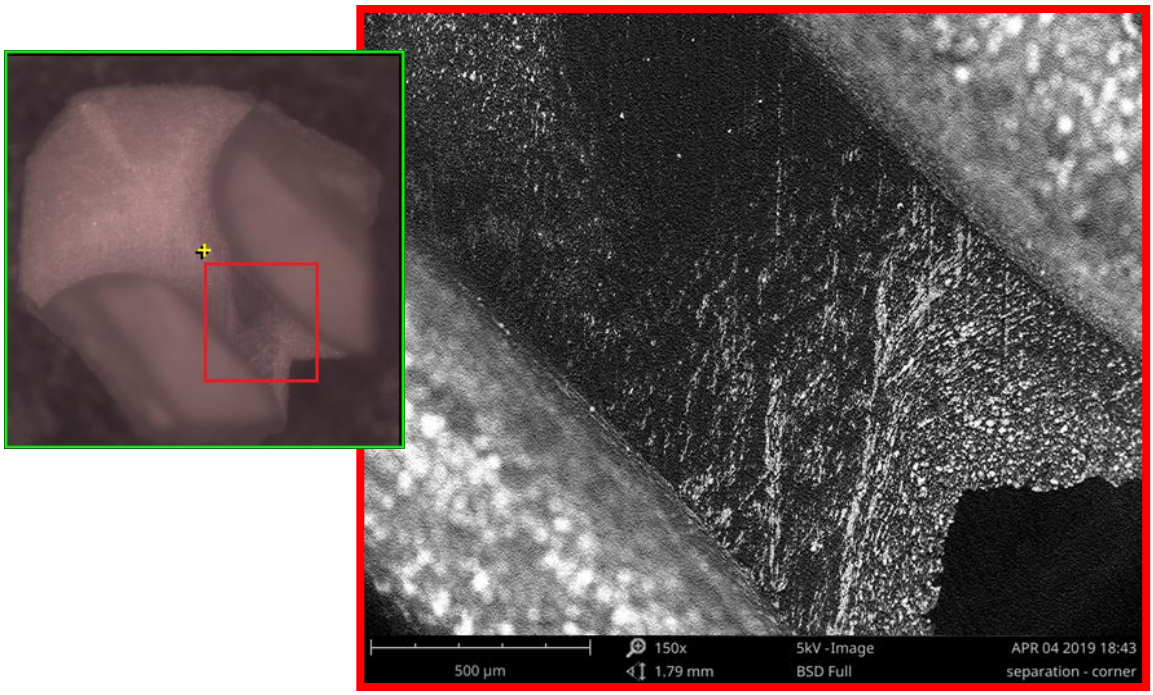

Fig. 37 - SEM selected mold element for phase separation of 17-4 PH feedstock

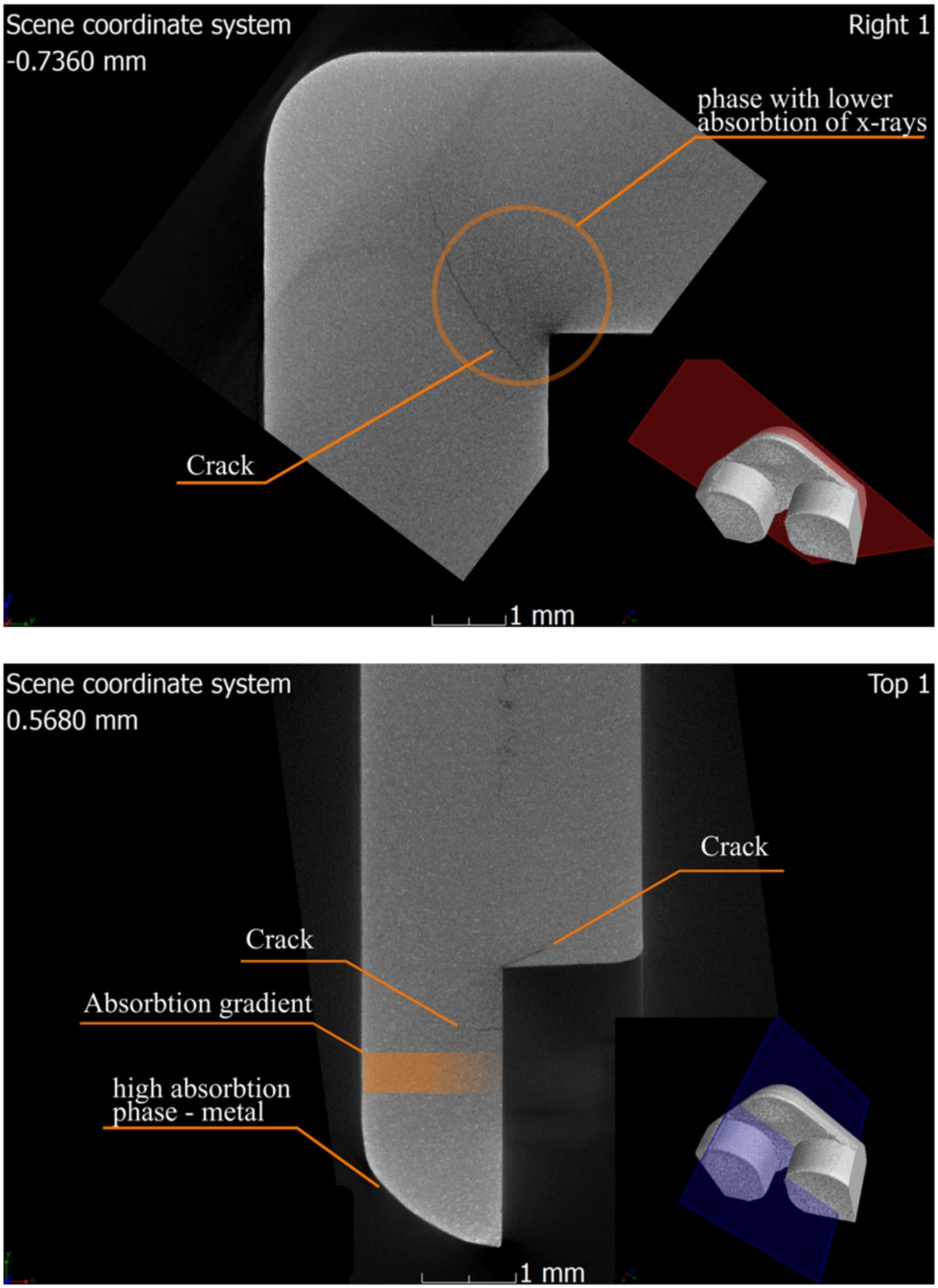

Fig. 38 - CT imaging of test sample

From the results of CT imaging, where X-ray absorption differs in thickness, it is evident that phase separation is not problem only on the surface, but it occurs in a bulk. Small absorption is at the corner, where exceed of binder is predicted due to shear rate gradient. Also, cracks, as accompanying effect of separation, are evident in Fig.38.

5.5 Mold Concept of Insert Mold

Specimens for tensile tests were molded at two modifications: without weld line, when only one gate has been used, and with weld line, when filling has been supported with a second gate.

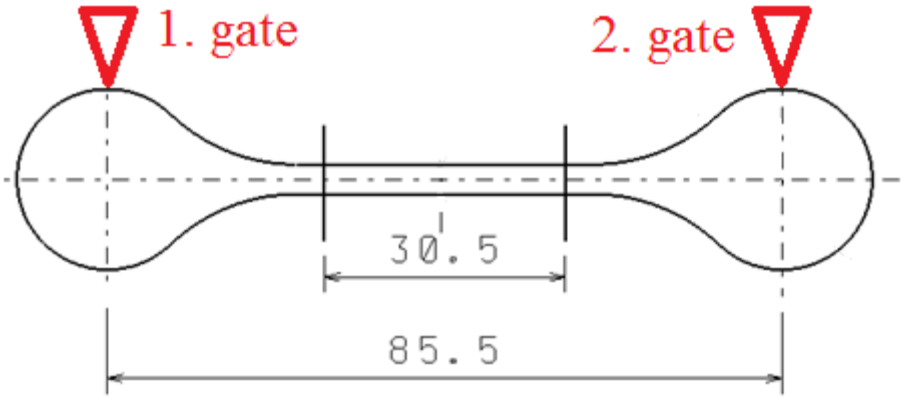

Fig. 39 - Gating possibilities in insert mold for tensile strength testing

Copper, aluminum alloy, and bronze inserts were machined by milling and drilling. Machining was performed in the laboratories of the Department of Production Engineering TBU. The tool paths were generated with NX CAM post-processor and outer dimensions of insert were tailored to IT5 tolerance.
Second group of inserts is based on polymers. 3D printed mold insert produced on Polyjet 3D printer with layer thickness of 25 microns was made of acrylic monomer with photoinitiator with post thermal treatment to increase HDT temperature up to 95 °C, when the specimen is loaded with 0.45 MPa. Another mold insert was produced by casting of epoxy resin compound (Fig. 40). First of all, the positive model was designed, and therefore 3D printed on Formlabs Form 2 3D printer from mixture of methacrylated oligomers, monomers and photoinitiator with 50μm layer thickness. After printing, the non-cured resin was washed in 99,5 % isopropyl alcohol for 10 minutes, and finally post-cured in 465 nm UV light for 2 hours. To this model, a silicon rubber was casted to obtain the negative copy. As a silicon material, Lukopren N1522 with 2 wt.% of activator of vulcanization due to high tear resistivity was chosen. Subsequently, pure epoxy resin and epoxy resin with thermal conductive filler were casted into the silicon mould. As a casting material for mold insert, high temperature resistant epoxy resin Gamod Fluid T206 with thermal conductive hexagonal boron nitride (hBN) has been used. According to low density of hBN, 15 wt. % (approx. 35 vol.%) of a filler has been used in the compound. This modification of resin with hBN increased the thermal conductivity for 148 %. Both PolyMIM 17-4PH and WPC compounds were utilized to test the influence of weld line on tensile strength.

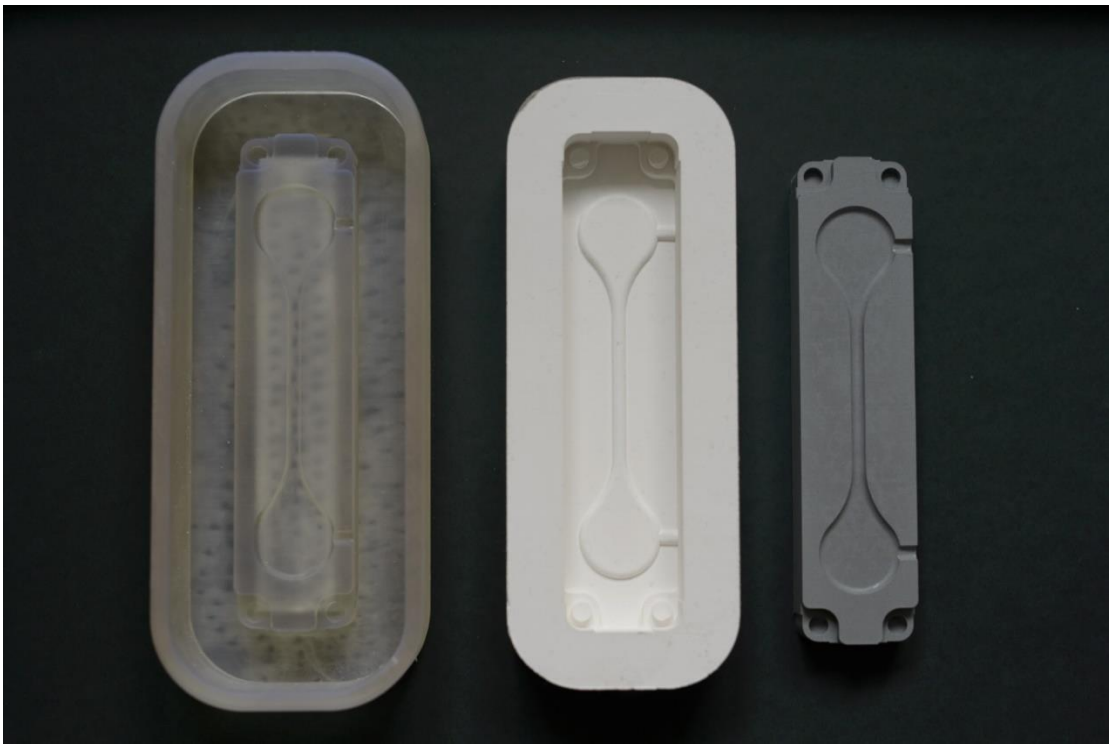

Fig. 40 - 3D printed model (left), negative silicon mold (middle), final insert from epoxy resin (right)

Overall mechanical and thermal properties of all mold inserts are summarized in Table 9.

Table 9 - Overall mechanical and thermal properties of mold inserts

Material of mold inserts		***R*m**			***λ***		
		[MPa]			[$W.m^{-1}.k^{-1}$]		
		$\bar{x}$	s	υ	$\bar{x}$	s	υ
Aluminium		453.5	22.6	5.0	383.90	14.86	3.87
Copper		167.3	12.7	7.6	154.03	2.16	1.40
Bronze		301.1	8.4	2.8	64.15	1.50	2.34
3D printed		54.2	3.7	6.8	0.992	0.015	1.54
epoxy resin	**+ 0 vol.% hBN**	47.3	12.8	27.1	0.389	0.007	1.70
	+ 35 vol.% hBN	21.4	4.1	19.2	0.204	0.008	3.66

5.6 Tensile strenght of molded highly filled compounds related to weld lines

Tensile test specimens molded in all inserts. In case of PIM compound (17-4PH feedstock), debinding and sintering was carried out prior mechanical testing. The results are summarized in Tables 10-13.

Table 10 - 17-4PH tensile strength for inserts without weld line

No.	Tensile Strength [MPa]					
	Copper	**Aluminium**	**Bronze**	**ER + hBN**	**ER**	**3D printer**
1	1080	1180	1180	1200	1170	1280
2	1110	1220	1230	1260	1160	1280
3	1080	1220	1190	1240	1240	1270
4	1090	1210	1270	1270	1210	1260
5	1100	1200	1130	1100	1190	1190
6	1080	1180	1170	1190	1230	1240
7	1090	1200	1180	1240	1230	1230
8	1130	1160	1250	1150	1230	1220
9	1040	1240	1230	1260	1210	1280
10	1080	1210	1240	1240	1190	1240
$\bar{x}$	1088	1202	1207	1215	1206	1249
$\tilde{x}$	1085	1205	1210	1240	1210	1250
S	23.48	23.48	43.47	55.03	27.57	30.35
Y	2.16	1.95	3.60	4.53	2.29	2.43

Table 11 - 17-4PH Tensile Strength for inserts with weld line

No.	Tensile Strength [MPa]					
	Copper	**Aluminium**	**Bronze**	**ER + hBN**	**ER**	**3D printer**
1	1180	1150	1140	1260	1260	1310
2	1240	1220	1280	1240	1180	1260
3	1170	1230	1190	1160	1170	1270
4	1210	1170	1170	1260	1140	1260
5	1230	1230	1230	1190	1230	1190
6	1240	1210	1190	1240	1220	1220
7	1150	1170	1250	1170	1170	1290
8	1150	1170	1230	1180	1230	1180
9	1190	1200	1190	1220	1240	1240
10	1200	1230	1250	1270	1260	1200
$\bar{x}$	1196	1198	1212	1219	1210	1242
$\tilde{x}$	1195	1205	1210	1230	1225	1250
s	34.06	30.48	42.90	40.95	41.90	43.67
υ	2.85	2.54	3.54	3.36	3.46	3.52

Table 12 - WPC Tensile Strength for inserts without weld line

No.	Tensile Strength [MPa]					
	Copper	**Aluminium**	**Bronze**	**ER + hBN**	**ER**	**3D printer**
1	22.2	26.4	24.5	26.3	28.5	28.2
2	22.7	26.4	21.2	28.7	27.3	30.0
3	23.0	24.3	23.9	25.8	26.9	28.7
4	20.1	27.8	21.0	27.4	29.3	28.5
5	20.8	24.9	22.1	27.3	27.6	27.8
6	21.6	27.0	24.9	27.8	27.9	29.3
7	22.4	28.3	23.8	26.8	26.8	30.4
8	21.6	22.3	23.0	25.2	26.9	30.1
9	20.8	26.2	23.2	28.2	27.5	27.0
10	21.2	26.7	25.3	28.5	26.3	28.9
$\bar{x}$	21.64	26.03	23.29	27.2	27.50	28.89
$\tilde{x}$	21.60	26.40	23.50	27.35	27.40	28.80
S	0.93	1.77	1.49	1.17	0.89	1.08
Y	4.31	6.80	6.38	4.29	3.23	3.75

Table 13 - WPC Tensile Strength for inserts with weld line

No.	Tensile Strength [MPa]					
	Copper	**Aluminium**	**Bronze**	**ER + hBN**	**ER**	**3D printer**
1	5.79	7.14	8.39	7.65	7.05	7.25
2	5.22	6.57	7.10	8.72	8.76	9.37
3	7.87	5.20	7.04	9.11	7.45	8.50
4	6.86	6.55	6.58	8.64	7.96	7.68
5	7.01	6.32	9.40	8.22	6.85	8.72
6	5.77	6.70	6.94	7.06	8.12	7.39
7	4.34	5.86	6.77	6.87	7.68	9.35
8	7.05	5.34	7.47	8.11	6.96	9.85
9	4.29	4.92	8.21	9.05	7.25	9.23
10	5.76	6.87	7.49	8.51	6.92	9.02
$\bar{x}$	5.99	6.14	7.53	8.19	7.50	8.63
$\tilde{x}$	5.78	6.43	7.28	8.36	7.35	8.87
s	1.19	0.77	0.88	0.78	0.63	0.91
υ	19.89	12.51	11.66	9.53	8.36	10.53

5.6.1 Outlier Test

Obtained data was inspected to the outlier value. Bellow, the analysis for the copper insert and PIM feedstock is calculated as the example.

$$G = \frac{\bar{x} - x_{\min}}{s} = \frac{1088 - 1040}{23.5} = 2.0425$$

From the Grubbs test can be claimed that the smallest data value 1040 MPa is 2.04 standard deviations less than mean of a sample data. After performing a 1-sample *t*-test on 10 observations, the inverse cumulative probability of which equals the critical value of 1.8331. According to the absolute value of Grubbs test $G = 2.0425$, which is higher than the *t*-statistic value (1.8331), it is possible to fail to reject the null hypothesis and conclude that the smallest value is not an outlier. The *p*-value (0.096) indicates that if the obtained data are from the same normally distributed population, the possibility of obtaining such small value is 9.6 %. This statistic has been done for all sample data of the population (Table 14).

Table 14 - Outlier tests statistics for 17-4PH and WPC with and without weld line

material	Cu	Al	Bronze	ER+hBN	ER	3D
17-4 PH	H_0	H_0	H_0	H_0	H_0	H_0
17-4 PH weld line	H_0	H_0	H_0	H_0	H_0	H_0
WPC	H_0	H_0	H_0	H_0	H_0	H_0
WPC weld line	H_0	H_0	H_0	H_0	H_0	H_0

It is possible to fail to reject the null hypothesis (*p*-value > α), and conclude that not enough evidence is available to suggest the null as false at the 95 % confidence level. If significance level was set to $\alpha = 10\%$ values in orange color will reject the null hypothesis and accept alternative.

5.6.3 Normality Test

Test of normal distribution was performed with Anderson-Darling method. Copper insert is analyzed as an example. Anderson-Darling is:

$$AD = -n - \frac{1}{n}\sum_{i=1}^{n}(2i-1)\left[\ln F(X_i) + \ln(1 - F(X_{n-i+1}))\right]$$

$F(X_i)$ and $1\text{-}F(X_{n+1-i})$ are values calculated from the standard normal cumulative distribution function, which arises when mean is 0, the standard deviation is 1, and *Si* is auxiliary function which formula is:

$$S_i = \sum_{i=1}^{n}(2i-1)\left[\ln F(X_i) + \ln(1 - F(X_{n-i+1}))\right]$$

Anderson-Darling statistic is therefore simplified to:

$$AD = -n - \frac{1}{n}\sum_{i=1}^{n} S_i \longrightarrow AD = -10 - \frac{-105.1184}{10} \longrightarrow AD_{adj} = 0.5118$$

According to small sample size Anderson-Darling statistic is adjusted to:

$$AD_{adj} = AD\left(1 + \frac{0.75}{n} + \frac{2.25}{n^2}\right) \longrightarrow AD_{adj} = 0.5118\left(1 + \frac{0.75}{10} + \frac{2.25}{10^2}\right) \longrightarrow AD_{adj} = 0.5617$$

Table 15 - Selection of correct formula (highlighted in green) for adjusted *AD* value

Anderson-Darling Statistic	Formula for p-value Calculation
$AD_{adj} \geq 0.60$	exp (1.2937-5.703(AD_{adj})+0.0186(AD_{adj})^2)
$0.34 < AD_{adj} < 0.60$	exp (0.9177-4.279(AD_{adj})-1.38(AD_{adj})^2)
$0.20 < AD_{adj} < 0.34$	1-exp (-8.318+42.796(AD_{adj})-59.938(AD_{adj})^2)
$AD_{adj} \leq 0.20$	1-exp (-13.436+101.14(AD_{adj})-223.73(AD_{adj})^2)

Therefore, *p-value* for small sample size is calculated as:

$$p - value = \exp\left(0.9177 - 4.279(\mathrm{AD}_{\mathrm{adj}}) - 1.38(\mathrm{AD}_{\mathrm{adj}})^2\right) = 0.1463$$

It is possible to fail to reject the null hypothesis (*p*-value > α), and conclude that not enough evidence is available to suggest the null as false at the 95 % confidence level.

The same principles of analysis were adopted for the remaining inserts and both PIM and WPC filled compounds, and the results of Anderson-Darling statistics is collected in Table 16.

Table 16 – Normality tests statistics for 17-4PH and WPC with and without weld line

material	Cu	Al	Bronze	ER+hBN	ER	3D
17-4 PH	H_0	H_0	H_0	H_0	H_0	H_0
17-4 PH weld line	H_0	H_0	H_0	H_0	H_0	H_0
WPC	H_0	H_0	H_0	H_0	H_0	H_0
WPC weld line	H_0	H_0	H_0	H_0	H_0	H_0

For all cases, the *p*-value is larger than the significance level α = 5%, the decision is to fail to reject the null hypothesis, and therefore, with the probability of 1-α the obtained data originates in normal distribution. If significance level was set to α = 10% values in orange color will reject the null hypothesis and accept alternative.

5.6.5 Test for Equal Variances

To do one-way ANOVA test, variances of the population have to be equal. Levene test was performed for tensile strength from copper insert with/without weld line as an example.

$$W = \frac{(N-k)}{(k-1)} \frac{\sum_{i=1}^{k} N_i (\overline{Z_{i.}} - \overline{Z}_{..})^2}{\sum_{i=1}^{k} \sum_{j=1}^{N_i} (Z_{ij} - \overline{Z}_{i.})^2} = \frac{(10-2)}{(2-1)} \frac{\sum_{i=1}^{k} N_i (\overline{Z_{i.}} - \overline{Z}_{..})^2}{\sum_{i=1}^{k} \sum_{j=1}^{N_i} (Z_{ij} - \overline{Z}_{i.})^2} = 2.5413$$

Upper critical value for *F*-distribution at significance level of α = 5 % with *k*-1 and *N*-*k* degrees of freedom is calculated as an inverse cumulative probability with result of

$$F_{\alpha,k-1,N-k} = F_{5\%,1,8} = 5.318.$$

When statistic of Levene test is lower than the upper critical value for *F*-distribution, it is possible to fail to reject the null hypothesis and not accept the alternative hypothesis. Therefore, it is not statistically significant evidence at α = 5 % to show that there is a difference in variances.
Test for Equal variances was performed same way for all remaining pairs of the data as for copper inserts. Overall results are shown in Table 17.

Table 17 – Test for equal variances for 17-4PH and WPC with and without weld line

material	Cu	Al	Bronze	ER+hBN	ER	3D
17-4 PH	H_0	H_0	H_0	H_0	H_0	H_0
WPC	H_0	H_0	H_0	H_0	H_0	H_0

For all instances the null hypothesis was fail to reject at the significance level α = 5 % and therefore, one-way ANOVA comparison of the tensile strength means will be performed.

5.6.7 One-way ANOVA

When sample data are from normal population and all variances are equal, One-way ANOVA for comparison of tensile strength from insert with and without weld line of the sample data means was done:

$$F = \frac{MST}{MSE}$$

where numerator and denominator are for coper inserts calculated as the example:

$$SST == \sum_{i=1}^{k} n(x_i - \bar{x})^2 = \sum_{i=1}^{k} 10(1088-1142)^2 + 10(1196-1142)^2 = 58320$$

$$MST = \frac{SST}{p-1} = \frac{58320}{2-1} = 58320$$

$$SSE = \sum_{i=1}^{k} (n-1)s_i^2 = (10-1)23.43^2 + (10-1)34.06^2 = 15400$$

$$MSE = \frac{SSE}{N-p} = \frac{15400}{20-2} = 855.55$$

$$F = \frac{MST}{MSE} = \frac{58320}{855,55} = 68.1667$$

Upper critical value for *F*-distribution at significance level of α = 5 % with *k*-1 = 1 and *N*-*k* = 8 degrees of freedom is calculated as an inverse cumulative probability with result of:

$$F_{\alpha,k-1,N-k} = F_{5\%,1,8} = 5.3177$$

Calculated test statistic for ANOVA method is higher than the critical value for *F*-distribution and also *p*-value for One-way ANOVA of tensile strength sample data means from cooper inserts with and without weld line is *P*-value = 0.00. Therefore, it is possible to reject the null hypothesis H_0 at the 0.05 significance level.

Table 18 – One-way ANOVA for 17-4PH and WPC with and without weld line

material	Cu	Al	Bronze	ER+hBN	ER	3D
17-4 PH	H_0	H_0	H_0	H_0	H_0	H_0
WPC	H_0	H_0	H_0	H_0	H_0	H_0

From the results of one-way ANOVA it is possible to see that the effect of weld line during injection molding of 17-4PH is statistically significant only when the copper insert was used. In case of conventional injection molding, weld line effect is significant regardless of used insert material.

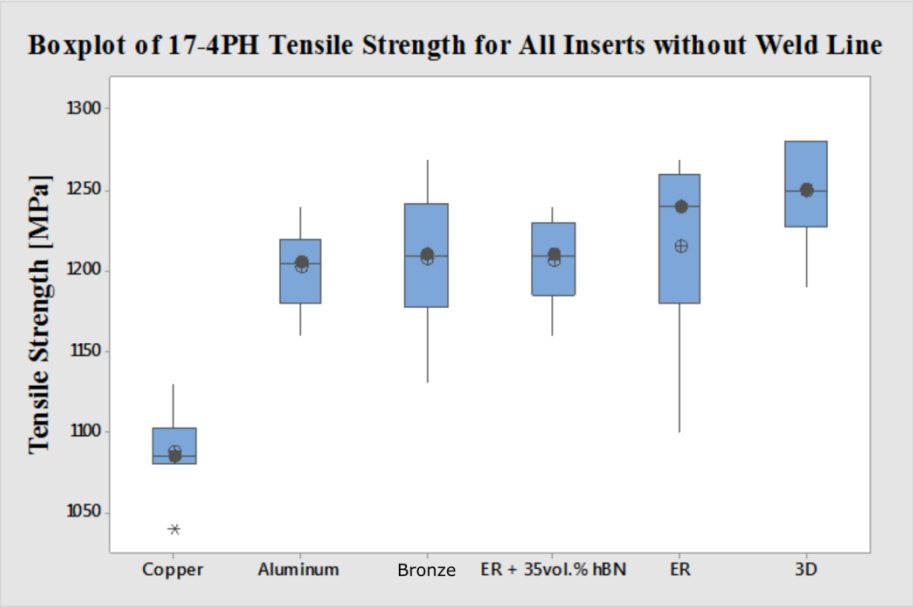

Fig. 41 - Boxplot of Tensile strength of 17-4PH for all insert without weld line

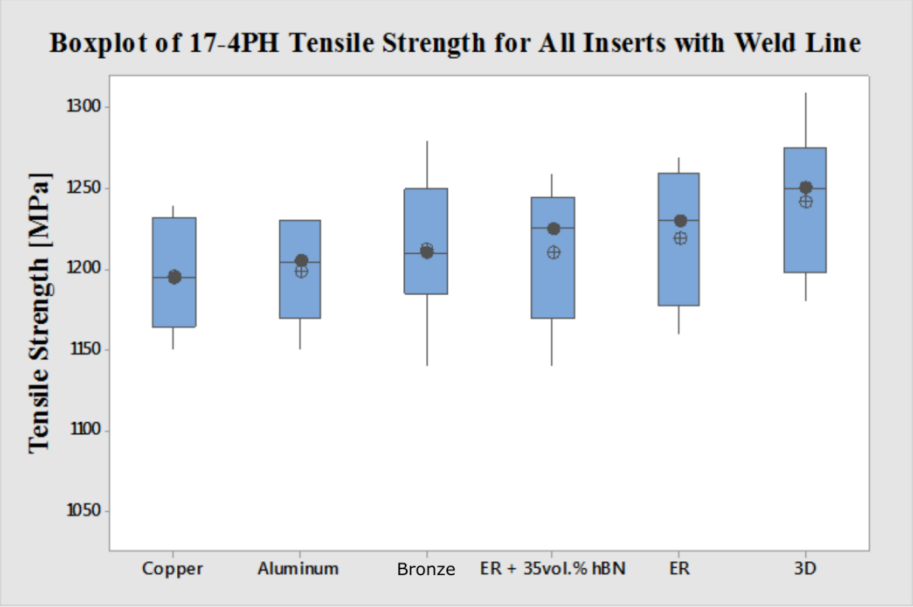

Fig. 42 - Boxplot of Tensile strength of 17-4PH for all insert with weld line

Influence of weld lines on tensile strength of 17-4PH compounds is not significantly affected by thermal conductivity of mold inserts (Rm,copper WL = 1196MPa, Rm, 3D WL = 1242 MPa). Increase of strength with slower cooling is about 4 %. On the other hand, when weld line is not formed, filling trajectory is longer and rapid solidification of 17-4PH feedstock due to high thermal conductivity results in lower tensile strength (Rm,copper = 1088MPa, Rm, aluminium = 1202MPa). Due to this finding, weld line formation has an effect of filling time reduction without a significant change of tensile strength.

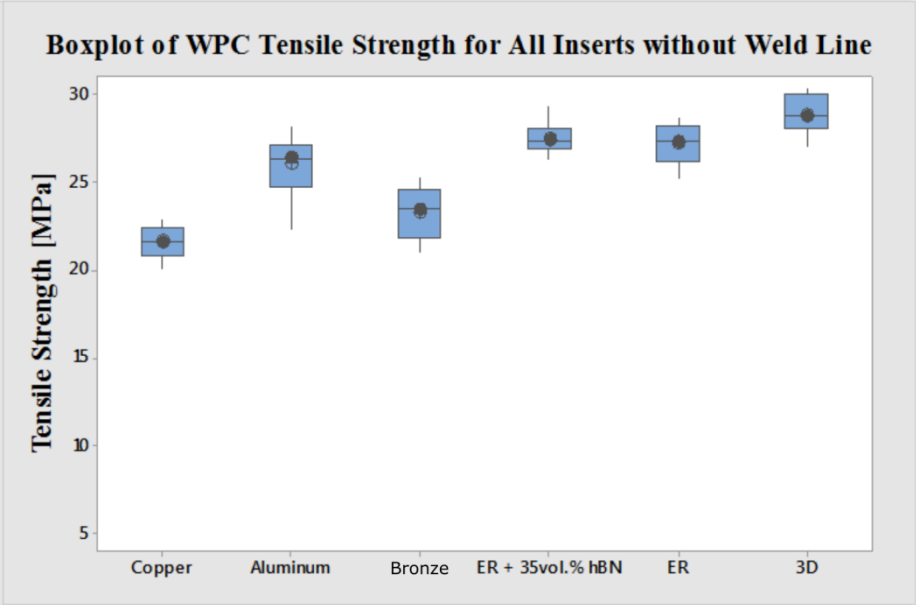

Fig. 43 - Boxplot of Tensile strength of WPC for all insert without weld line

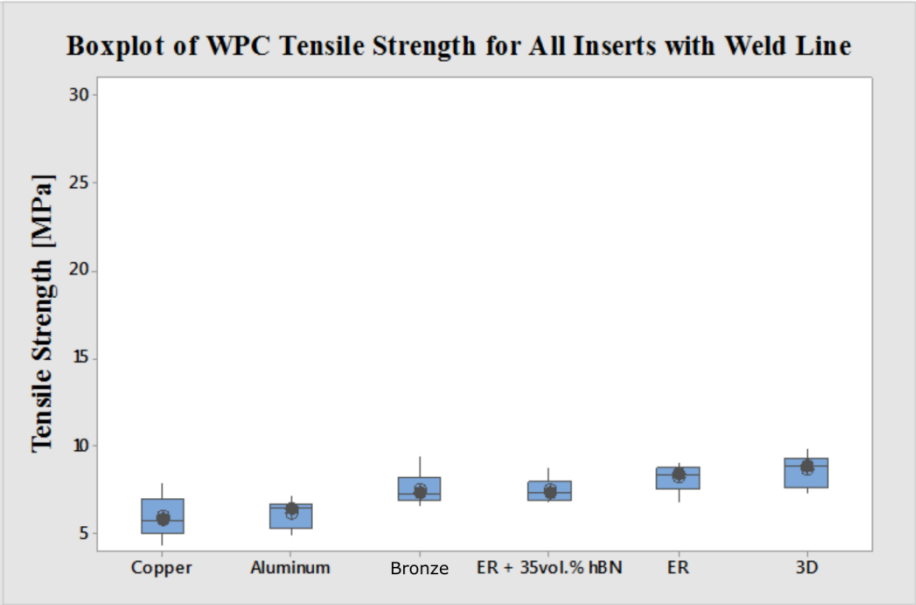

Fig. 44 - Boxplot of Tensile strength of WPC for all insert with weld line

On the other hand, from the boxplot diagrams (Figs. 43, 44) it is evident that cooling rate has effect on tensile strength of WPC compounds. When polymeric insert (λ = 0.2 W.m-1.k-1) is used instead of copper (λ = 394 W.m-1.k-1), tensile strength is for 33 % higher (Rm,copper = 21.64MPa, Rm, 3D = 28.89 MPa). Further, thermal conductivity affects tensile strength when weld line is formed. Positive effect of inserts with low cooling rate is up to 45 % (Rm,copper WL = 5.99MPa, Rm, 3D WL = 8.63MPa). Therefore, slower cooling rate results in higher tensile strength. Higher tensile properties are also result of elongated effect of packing due to slower solidification of the smallest cross section profile, for this case - gating system, that is confirmed with increased tensile strength in case of no weld line.

CONCLUSION

Presented Doctoral Thesis deals with mold design concept for injection molding of highly filled materials, where experiment is divided into two sections - mold design is studied from the perspective of phase separation and weld line formation.

Materials examined were 17-4PH stainless steel feedstock employed in powder injection molding (PIM) and wooden plastic composite (WPC) based on high density polyethylene matrix. As initial characteristics, melt rheology and thermal properties were determined and considered in Moldflow simulations.

With respect to previous findings in the area of phase separation, injection molding was simulated for two testing geometries, where shear rate gradient was found as a good indicator of phase separation. Injection molding is a processing route typical for complex shapes of molded parts, where the cross section changes often take place. For this reason, the new testing geometry for phase separation was designed, and an approach to determine the phase separation was developed.

Further, taking into account the fact that the main cause of phase separation are shear rate gradients, the monitoring of temperature may be useful in qualification of phase separation. To measure the temperature inside a mold cavity, non-conventional infrared sensors in 6 locations were tested. This method allows on-line monitoring of phase separation, which may be eventually inducted by deterioration of a cavity surface due to a wear associated with changes in melt/mold interactions, surface energy, and roughness.

The presence of the phase separation, after overheating of the material due to the shear rate gradients, was confirmed also with the help of computed tomography. According to the previous studies, observed cracks may lead to delamination after sintering, which is also accompanying phenomenon of the phase separation.

Highly filled materials are susceptible to negative effect of weld lines on tensile strength of molded parts. Weld line strength may be increased with increased time and temperature of diffusivity. For this reason, mold inserts for tensile test specimens from various thermal conductivity materials were designed and produced. Weld line formation has a strong influence on the tensile strength of WPC composites. When the acrylic polymer printed insert was used, the weld line strength reached the about 45 % higher in comparison with the copper insert. Enhanced tensile properties result also from the elongated effect of packing due to slower solidification of the smallest cross section profile. Situation differs in case of PIM feedstock, where the effect of weld lines is noticeable only for copper insert. However, the effect of weld line is positive in this case. The trajectory during injection molding of samples without weld line was longer in comparison to the situation when two gates were utilized (and weld line occured). PIM feedstock (λ = 4.0 $W.m^{-1}.k^{-1}$) in combination with copper insert (λ = 394 $W.m^{-1}.k^{-1}$) solidifies quickly, and therefore, the elongation of filling stage (one gate -

without weld line) results in the decreased packing time leading into deteriorated tensile strength. For this reason, weld lines in PIM technology may be advantageously used with regard to tensile strength properties, when filling time is decreased and duration of packing stage may be elongated.

CONTRIBUTION TO SCIENCE AND PRACTICE

The Thesis is aimed on qualification of phase separation during injection molding when material may be regrinded and used again. In other words, the aim is to enhance production economic with on-line determination of phase segregation. For this point of view contribution of the Doctoral Thesis to science and practice is:

- new testing geometry for phase separation with combination of segregation supporting elements;
- verification of reason for phase separation with CAE simulations where shear rate gradients take place;
- proposed way to measure melt temperature inside mold cavity and ensure identification of potentially critical area, where phase separation may occur due to dissipation heat induced by shear rate;
- non-destructive qualification of phase separation by computed tomography with respect to qualification in bulk.

Design standards for PIM tooling are generally copying design standards for conventional injection molding. When highly filled compounds are molded to form complex shapes, weld lines may occur. From the second part of the Thesis, the contribution to science and practice includes:

- weld lines in conventional injection molding of highly filled compound strongly affect tensile strength of molded products;
- thermal conductivity of mold insert in conventional injection molding of highly filled compounds has significant effect on tensile strength, where slower cooling rate have positive effect;
- weld lines in PIM do not effect tensile strength of final (sintered) products
- thermal conductivity of mold inserts in PIM has insignificant influence on tensile strength.

With the respect to the current competitor of forming technologies - additive manufacturing, the Thesis opens a possibility of low volume injection molding where:

- 3D printed mold inserts might be used;
- silicon mold copying 3D printed master model may be used, where liquid polymeric system with thermally conductive filler (to increase thermal conductivity) is casted to form a mold insert.

REFERENCES

Andrews, I., et. al., (2010) *A Case Study on Computational Fluid Dynamics Analysis of Micro-MIM Products.* Powder Injection Moulding International, 4, pp. 55-65.

Atre, S., V., Park, S., J., Zauner, R., German, R., M. (2007) *Process Simulation of Powder Injection Molding. Identification of Significant Parameters During the Mold Filling Phase.* Powder Metallurgy, 50 (1), pp. 76-85.

Barriere, T., Gelin, J. C., Liu, B. (2002) *Improving Mould Design and Injection Parameters in Metal Injection Moulding by Accurate 3D Finite Element Simulation.* Journal of Materials Processing Technology, 125-126, pp. 518-524.

Bendada, A., Derdouri, A., Lamontage, M., Simard, Y. (2004) *Analysis of thermal contact resistance between polymer and mold in injection molding.* Applied Thermal Engineering, 24, pp. 2029-2040.

Biehl, S., Lűthje, H., Bandorf, R., Sick, J. H. (2006) *Multifunctional thin film sensors based on amorphous diamond-like carbon for use in tribological applications,* Thin Solid Films, 515, pp. 1171-1175.

Biehl, S. et. al. (2016) *Multifunctional thin film sensor system as monitoring system in production*. Microsystem Technologies, 22, pp. 1757-1765.

Bilovol, V., V., Kowalski, L., Duszczyk, J., Katgerman, L. (2003a) *Comparison of numerical codes for simulation of powder injection moulding.* Powder Metallurgy, 46 (1), pp. 55-60.

Bilovol, V., V. (2003b) *Mould filling simulations during powder injection moulding.* Ph.D. Thesis, Delft University of Technology, Delft, The Netherlands.

Chen, S. C., Chen, J. T., Chien, D. R., Chen, C. S. (2007) *Investigation on the weldline strength of thin-wall injection molded ABS parts.* International Communications in Heat and Mass Transfer, 34 (4), pp. 448-455

Chen, S. C., et. al. (2009) *Effect of cavity surface coating on mold temperature variation and the quality of injection molded parts*. International Communications in Heat and Mass Transfer, 36 (10), pp 1030-1035.

Chookaew, W. (2013) *An Investigation of Weldline Strength in Injection Molded Rubber Parts*. Energy Procedia, 34, pp 767-774.

Drummer, D., Messingschlager, S. (2014) *Ceramic injection molding material analysis, modeling and injection molding simulation.* AIP Conference Proceedings, pp. 582 - 586

Duretek, I., Holzer, C. (2017) *Material Flow Data for Numerical Simulation of Powder Injection Molding.* Universal Journal of Materials Science, 5, pp. 7-14.

German, R. M., Bose, A. (1997) *Injection molding of metals and ceramics*. [1st ed.]. Princeton: Metal Powder Industries Federation, 413 p. ISBN 1-878-954-61-x.

German, R. M. (2013) *Powder Injection Molding Design & Applications,* Innovative Materials Solutions, 260 p. ISBN 978-0972764209

German, R.M., 2011. *Metal injection molding: a comprehensive MIM design guide*, Princeton: Metal Powder Industries Federation, 194 p. ISBN 978-0-98194966-6

Hausnerova, B., Marcanikova, L., Filip, P., Saha P. (2011a). *Optimization of powder injection molding of feedstock based on aluminium oxide and multicomponent water-soluble polymer binder*. Polymer Engineering & Science, 51 (7), pp. 1376-1382.

Hausnerova, B. (2011b). *Powder Injection Molding – An Alternative Processing Method for Automotive Items*, New Trends and Developments in Automotive Systems Engineering, pp. 130-146.

Hausnerova, B., Sanetrnik, D., Ponizil, P. (2013). *Surface structure analysis of injection molded highly filled polymer melts*, Polymer Composites, 34, pp. 1553–1558.

Heaney, D. F. (2012). *Handbook of metal injection molding*. Oxford: Woodhead Publishing, 2012, xvi, 586. Woodhead Publishing in materials. ISBN 978-0-85709-066-9.

Hsu, K. C., and P. C. Tsai. (1995) *Spiral Flow Analysis on the Injection Molding of Alumina Powder – An Experimental Design*, Ceramics International, 21 (6), pp. 439-443

Jain, A. K., Murty, M. N., Flynn, P. J. (1999) *Data Clustering: a Review,* ACM Computing Surveys, 19 (3), pp. 264-323.

Jenni, M. (2008) *Quantitative study of powder binder separation of feedstock*, PIM International, 2 (4), pp. 50-55

Jenni, M., Zauner, R., Stampfl, J. (2009) *Measurement Methods for Powder Binder Separation in PIM Components*. In EURO PM 2009: Proceedings Vol 2. Copenhagen: European Powder Metallurgy Association, pp. 141-146. ISBN 978-1899072071.

Jiranek, L., Hausnerova, B., Hartwig, T. (2010) *Community Design 001704974*, Office for Harmonization in the Internal Market, Alicante.

Karatas, Ç., Sözen, A., Arcaklioglu, E., Erguney S. (2008) *Investigation for mouldability for feedstocks used powder injection molding*. Materials & Design, 29 (9), pp. 1713-1724.

Kate, K. H., Enneti, R. K., McCabe, T., Atre, S. V. (2016) *Simulations and injection molding experiments for aluminum nitride feedstock.* Ceramics International, 42 (1), pp. 194-203.

Kistler (2019) *Pressure and Temperature Sensor, direct measuring ø4 mm.* [ref. 2018-04-12], available at: https://www.kistler.com/en/product/type-6190c/

Kyas, K, Cerny, J., Stanek., M., Manas, M., Manas, D. (2012) *Measuring of temperature and pressure in injection mold.* International Journal of Mathematics and Computers in Simulation, 6, pp. 600-607.

Marhöfer, M. (2016) *Validation of precision powder injection molding process simulations using a spiral test geometry.* AIP Conference Proceedings.

Martinsen, K., Gellein, L. T., Boivie, K. M. (2017) *Sensors embedded in surface coatings in injection moulding dies.* Procedia CIRP, pp. 386-390.

Thornagel, M. (2009) *MIM-Simulation: A Virtual Study on Phase Separation*. In EURO PM 2009: Proceedings Vol. 2. Copenhagen : European Powder Metallurgy Association, pp. 135-140. ISBN 978-1899072071.

Thornagel, M. (2010) *Simulating flow can help avoid mould mistakes*., Metal Powder Report, 65 (3), pp. 26-29

Walale, A., et. al. (2018) *Analysis of Shrinkage & Warpage in Ceramic Injection Molding of HPT Vane Leading Edge Core of a Gas Turbine Casting.* Materials Today: Proceedings, 5 (9), pp.19471-19479.

Walcher H. (2013) Personal Communication with Hartmut Walcher, MIM Expert in Arburg GmbH + Co KG.

Xie, L. et. al. (2010) *Influence of Particle Concentration and Type on Flow, Thermal, and Mechanical Properties of Wood-Polypropylene Composites.* Journal of Reinforced Plastics and Composites, 29 (13), pp. 1940-1951.

Yang, S., Zhang, R., Qu, X. (2015) *Optimization and evaluation of metal injection molding by using X-ray tomography*. Materials Characterization, 104, pp. 107-115.

Zhou, Y., Mallick, P. K. (2014) *Effect of Melt Temperature and Hold Pressure on the Weld-Line Strength of an Injection Molded Talc-Filled Polypropylene*. Journal of Composites, pp 1-8.

LIST OF FIGURES

LIST OF TABLES

AKNOWLEDGEMENTS

At this place I would like to express my sincere gratitude to my supervisor prof. Berenika Hausnerová for her help, time, advices and consultations. In addition, I would like to thank to assoc. prof. Vladimír Pata for his help with statistical evaluation of data and advices.
Further, I am deeply thankful for the support to my family, my friends, my colleagues and people who I met during my study.

LIST OF SYMBOLS

PIM	Powder Injection Molding
MIM	Metal Injection Molding
DSC	Differential Scanning Calorimetry
WLF	Williams-Landel-Ferry
IR	Infra-red
MF	Moldflow
SEM	Scanning Electron Microscopy
EDX	Energy-dispersive X-ray spectroscopy
CAD	Computer-aided design
CAE	Computer-aided engineering
PSH	Powder Space Holder
hBN	Hexagonal Boron Nitride
HDPE	High-density Polyethylene
PP	Polypropylene
ABS	Acrylo butadiene styrene
WPC	Wood-plastic composite
TiN	Titanium nitride
L/D	Length to diameter ratio
HRC	Rockwell hardness
mm	millimeter
μm	micrometer
g	gram
W	Watt
m	metre
K	Kelvin degree
°C	Celsius degree
V	Volt
%	percent
h	hour
min	minute
Pa	Pascal
MPa	Megapascal
s	second
vol.%	volume percent
wt.%	weight percent
D_e	Elastic stiggness
E	Young modulus
ν	Coefficient of variation
ρ	Density
p	Pressure

t	Time
Δ	Delta (difference)
λ	Thermal conductivity
δ	Shrinkage
$\bar{x}$	Arithmetic mean
$\tilde{x}$	Median
s	Standard deviation
α	Significance level
G	Grubbs test
AD	Anderson-Darling test
H_0	Null hypothesis
$H_{alternative}$	Alternative hypothesis
€	EURO
η	Shear viscosity
η_0	Shear viscosity of first newtonian plateau
τ	Shear stress
$\dot{\gamma}$	Shear rate
τ^*	Shear stress (transition - first plateau and shear thinning region)
n	Non-Newtonian index / number of observation
m	coefficient of consistency
N	Number of observations
k	sub-group
φ	Volume fraction of a filler
x, y, z	Cartesian coordination system
V_{ef}	Effective velocity
V_s	Velocity of solid phase
V_f	Velocity of fluid phase

LIST OF AUTHOR`S PUBLICATIONS

HUBA, J., SANETRNIK, D., HNATKOVA, E., HAUSNEROVA, B. Mechanical properties of sintered PIM test specimens. In: EAN 2014 - 52nd International Conference on Experimental Stress Analysis. Mariánské Lázně: Curran Associates, Inc., 2014

HAUSNEROVA, B., **HUBA, J.** Discrepancies in Design Determination of Metal Injection Molded Tensile Test Specimens. Development in Machining Tehcnology, Krakow, 2014, ISBN 978-83-7242-765-6.

HUBA, J., HAUSNEROVA, B. A New Mold Design For Qualification Of Powder/Binder Separation In Pim Technology. In: M2D2015: Proceedings of the 6th International Conference on Mechanics and Materials in Design. P Delgada: INEGI-FEUP, 2015, s. 559-562.

HUBA, J., HAUSNEROVA, B. A New Mold Design For Qualification Of Powder/Binder Separation In Pim Technology. In: M2D2015: Proceedings of the 6th International Conference on Mechanics and Materials in Design [online]. P Delgada: INEGI-FEUP, 2015, s. 559-562.

HUBA, J., SANETRNIK, D., HNATKOVA, E., HAUSNEROVA, B., DVORAK, Z. New application of powder injection molded product in medical field. Manufacturing Technology. 2016, vol. 16, iss. 1, s. 94-98. ISSN 1213-2489

FOJTL, L., **HUBA, J.**, KUBISOVA, M., PATA, V., MRACEK, A., SEDLACEK, T. Modern types of PVD/PACVD coatings used for injection molds and their effects on selected physical properties of mold cavities. In: METAL 2017 - 26th International Conference on Metallurgy and Materials, Conference Proceedings. Brno: TANGER Ltd., 2017, s. 1258-1263.

Utility models

HAUSNEROVA, B., **HUBA, J.**, KREIZLOVA, J. Vstřikovaná struktura pro kvalitativní vyhodnocení fázové separace kompozitu na bázi polymerní matrice vysoce plněné kovovým nebo keramickým práškem. IPC: Czech Republic. Utility model, CZ 2014-30495 U1

HUBA, J., HAUSNEROVA, B., PATA, V., HAUSNER, D. Vstřikovací forma. IPC: Czech Republic. Utiliti model, PUV 2019-36080 - *application filed*

AUTHOR`S CV

PERSONAL INFORMATION Jakub Huba

Pod Vrskom 7, 034 03 Ruzomberok (Slovakia)
+420 57 603 5173
+420 776 576 106
jhuba@utb.cz

WORK EXPERIENCE

2018 - Present — Assistant
Tomas Bata University in Zlin
nam. T. G. Masaryka 5555, 760 01 Zlin (Czech Republic)
www.utb.cz

2013–2018 — R&D Assistant
Plastic Cluster z.s.
Vavreckova 5262, 760 01 Zlin (Czech Republic)
www.plastr.cz
3D technologies (3D printing, 3D scanning)
evaluation of CT data

2013–2017 — Junior Researcher
Tomas Bata University in Zlin
nam. T. G. Masaryka 5555, 760 01 Zlin (Czech Republic)
www.utb.cz

EDUCATION AND TRAINING

2013–2019 — PhD. student
Tomas Bata University in Zlin, Zlin (Czech Republic)
Degree Programme: Process Engineering
Degree Course: Tools and Processes

2011–2013 — Ing.
Tomas Bata University in Zlin, Zlin (Czech Republic)
Degree Programm: Process Engineering
Degree Course: Technological Equipment Construction
Master's thesis: Mechanical Properties of Injection Molded Rubber Products

2008–2011 **Bc.**

Tomas Bata University in Zlin, Zlin (Czech Republic)

Degree program: Process Engineering
Degree course: Technological Equipment
Bachelor's thesis: Utilization of Reverse Engineering for Design of Injection Molds

PERSONAL SKILLS

Mother tongue(s) Slovak

	Listening	Reading	Spoken interaction	Spoken production	Writing
English	B2	B2	B2	B2	B2

Job-related skills
- Understanding of processes in plastic industry
- Good knowledge of tool design for plastic processing (especially of injection molds)
- Proactive in problem-solving

Digital skills
Microsoft Office ™ Tools
CAD, CAE, CAM programs (CATIA, Solid Works, Autodesk Moldflow, Cadmould, NX 9.5)
FEM/FEA programs (Cosmos, CATIA FEM modul)
VG StudioMAX 2.2 (Evaluation od CT data)
Graphic programs (Photoshop, Inkscape, Keyshot)

Driving licence B1, B

ADDITIONAL INFORMATION

Projects
- CORNET - Smart coating systems for process control and increased wear resistance in processing of natural fibre reinforces polymers - CZ.01.1.02/0.0/0.0/15_007/0001161
- Centre of advanced polymer and composite materials (Centers of Competence) - 2012-2019 - TE01020216
- Centre of Polymer Systems - (CZ.1.05/2.1.00/03.0111)

Jakub Huba

Mold Design Concept for Injection Molding of Highly Filled Compounds

Koncept vstřikovací formy pro vysoce plněné polymery

Doctoral Thesis Summary

Published by: Tomas Bata University in Zlín,

nám. T. G. Masaryka 5555, 760 01 Zlín.

Edition: published electronically

Typesetting by: Jakub Huba

This publication has not undergone any proofreading or editorial review.

Publication year: 2019

First Edition

ISBN 978-80-7454-852-9